AD-A161 968 DESIGN OF A 10 GHZ 10 MW GYROTRON(U) NAVAL RESEARCH LAB 1/1
WASHINGTON DC M E READ ET AL. 27 NOV 85 NRL-MR-5629

UNCLASSIFIED F/G 9/5 NL

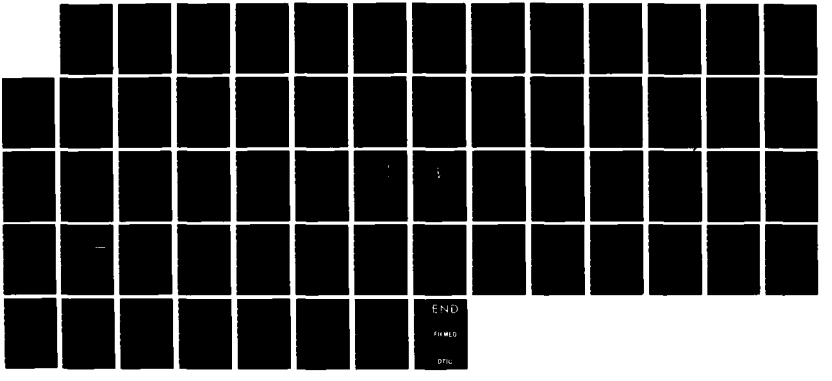

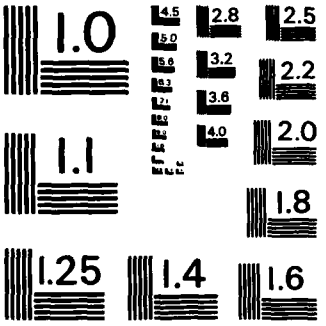

NRL Memorandum Report 5629

Design of a 10 GHz, 10 MW Gyrotron

M. E. READ AND G. BERGERON*

High Power Electromagnetic Radiation Branch
Plasma Physics Division

**JAYCOR, Inc.*
Alexandria, VA 22304

November 27, 1985

NAVAL RESEARCH LABORATORY
Washington, D.C.

SECURITY CLASSIFICATION OF THIS PAGE

REPORT DOCUMENTATION PAGE

AD-A160 968

1a REPORT SECURITY CLASSIFICATION: UNCLASSIFIED	1b RESTRICTIVE MARKINGS
2a SECURITY CLASSIFICATION AUTHORITY	3 DISTRIBUTION / AVAILABILITY OF REPORT: Approved for public release; distribution unlimited.
2b DECLASSIFICATION / DOWNGRADING SCHEDULE	
4 PERFORMING ORGANIZATION REPORT NUMBER(S): NRL Memorandum Report 5629	5. MONITORING ORGANIZATION REPORT NUMBER(S)
6a. NAME OF PERFORMING ORGANIZATION: Naval Research Laboratory; 6b OFFICE SYMBOL (If applicable): Code 4740	7a. NAME OF MONITORING ORGANIZATION
6c. ADDRESS (City, State, and ZIP Code): Washington, DC 20375-5000	7b. ADDRESS (City, State, and ZIP Code)
8a. NAME OF FUNDING / SPONSORING ORGANIZATION: Walter Reed Army Med. Center; 8b. OFFICE SYMBOL (If applicable)	9. PROCUREMENT INSTRUMENT IDENTIFICATION NUMBER
8c. ADDRESS (City, State, and ZIP Code): Washington, DC 20012	10 SOURCE OF FUNDING NUMBERS: PROGRAM ELEMENT NO. / PROJECT NO / TASK NO. / WORK UNIT ACCESSION NO. DN480-884

11 TITLE (Include Security Classification): Design of a 10 GHz, 10 MW Gyrotron

12 PERSONAL AUTHOR(S): Read, M.E. and Bergeron, G.*

13a. TYPE OF REPORT	13b. TIME COVERED	14 DATE OF REPORT (Year, Month, Day)	15. PAGE COUNT
Interim	FROM 8/84 TO 6/85	1985 November 27	62

16 SUPPLEMENTARY NOTATION: *JAYCOR, Inc., Alexandria, VA 22304

17 COSATI CODES			18 SUBJECT TERMS (Continue on reverse if necessary and identify by block number)
FIELD	GROUP	SUB-GROUP	Relativistic gyrotron High power microwave generation

19 ABSTRACT (Continue on reverse if necessary and identify by block number)

A design for a 10 GHz, 10 MW gyrotron with a pulse length up to 100 microseconds has been realized and is discussed. Details of the cavity and the magnetron injection gun used to generate the electron beam are given. Consideration is given to cavities and beams suitable for producing radiation in the $TE_{1,3}$ and $TE_{1,4}$ modes. Conceptual designs for the collector and output window are also discussed.

20 DISTRIBUTION / AVAILABILITY OF ABSTRACT	21 ABSTRACT SECURITY CLASSIFICATION
☒ UNCLASSIFIED/UNLIMITED ☐ SAME AS RPT ☐ DTIC USERS	UNCLASSIFIED
22a NAME OF RESPONSIBLE INDIVIDUAL: M. E. Read	22b TELEPHONE (Include Area Code): (202) 767-4004; 22c. OFFICE SYMBOL: Code 4740

DD FORM 1473, 84 MAR — 83 APR edition may be used until exhausted. All other editions are obsolete.

SECURITY CLASSIFICATION OF THIS PAGE

CONTENTS

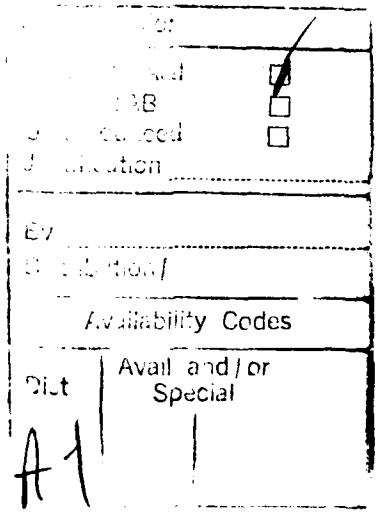

DESIGN OF A 10 GHz, 10 MW GYROTRON

Introduction

Gyrotrons with pulse lengths of one microsecond or longer have been widely developed for production of high power radiation at mm wavelengths[1]. This illustrates the great advantage that the gyrotron has over conventional high power sources for wavelengths less than one centimeter. However, for production of powers exceeding 1 MW, the utilization of highly overmoded cavities should make the gyrotron useful at lower frequencies. With very short pulses (30 ns), 1.5 GW and 25 MW has been produced at ~ 3 GHz and ~ 10 GHz respectively.[2,3] To date, however, no gyrotron with a pulse length of a microsecond or greater (therefore using a thermionic cathode) with a power significantly over 1 MW has been reported. In this paper, we discuss the design of a gyrotron for production of 10 MW at a frequency of 10 GHz, with a pulse length of up to 100 microseconds.

Manuscript approved September 24, 1985.

Basic Considerations

The most common form of a gyrotron is a circular cavity through which is passed an annular electron beam produced by a magnetron injection gun. This configuration has been well tested,[1] with the annular beam being particularly suited to the production of high power. This basic configuration was therefore chosen for this design.

Cavity Mode

Several types of cavity modes have been used successfully in high power gyrotron oscillators. All are TE modes, as is appropriate for the cyclotron maser interaction.[4] Significant research has been performed in the U.S. on $TE_{0,n}$ modes, and powers to 475 kW have been produced at 35 GHz.[5] However, while these modes, because of their low ohmic losses, appear to be particularly suited to CW power production at mm wavelengths[6], extrapolation to substantially higher powers is expected to be limited by mode competition.[5]

Whispering gallery ($TE_{m,1}$ or $TE_{m,2}$ modes with $m \gg 1$) have been used in the USSR for production of powers to 1.1 MW at 100 GHz[7]. Even with large values of m, these modes are largely free from mode competition, particularly at voltages less than 100 kV. Their principal disadvantage is that the transverse mode pattern, shown in Figure 1(a), is not suitable for radiation of a near-uniform, linearly polarized beam without fairly cumbersome mode conversion.[8] For the device of this paper, which is to be a general purpose source, this disadvantage was judged to be serious.

$TE_{1,n}$ modes, however, have the maximum electric field on center, and are nearly linearly polarized, as shown in Figure 1(b). In addition, high order modes ($n > 1$) can be easily transformed to a $TE_{1,1}$ mode via a fairly simple

waveguide converter.[9] The $TE_{1,n}$ mode will radiate as a nearly Gaussian mode from a simple horn. As with $TE_{0,n}$ modes, $TE_{1,n}$ modes can be severely affected by mode competition. However, for $TE_{1,n}$ modes there is evidence[3] that the cavity cross section can be deformed and/or split in order to decrease mode competition. Very high peak powers have been achieved with $TE_{1,n}$ modes, with 25 MW at 10 GHz having been reported for a gyrotron with a pulse length of 30 nanoseconds.[3] There is no apparent reason why a device with longer pulse lengths could not readily be realized with appropriate technology. Therefore, this type of mode was chosen for the device under consideration.

To determine the radial eigennumber, n, approximate calculations of the efficiency and power for various modes were made. These calculations were made by scaling from numerical integrations[10] of electron orbits through a low order mode cavity in which the axial field profile is approximated by a sinusoid. This technique has been previously established[11] to yield conservative results for the power and efficiency. In all of the calculations, a cavity of optimum length for a given beam voltage was assumed, as shown in Figure 2. The cavity quality factor Q was assumed to be twice the minimum (diffraction) $Q = Q_D \equiv 4\pi (L/\lambda)^2$ where L is the length of the cavity and λ is the wavelength. Changes from the nominal values of L and Q can be made to increase or decrease the output power, with some loss in efficiency occurring with changes in the length or for substantially lower values of Q.

The results of the calculations are shown in Figure 3, where the output power, as a function of beam voltage for various $TE_{1,n}$ modes is plotted. As can be seen, for beam voltages of 200 kV - 300 kV, (a range for which high voltage technology is well developed) the $TE_{1,3}$ and $TE_{1,4}$ modes can be used to produce the required 10 MW. As will be discussed below, there are tradeoffs in the expected performances of the two modes, primarily in efficiency,

operating Q, and mode competition. Therefore, both modes have been analyzed in some detail, as have the electron guns needed to produce the appropriate electron beams. The results of these analyses are described in the following sections.

Electron Gun Design

Choice of configuration

In a gyrotron, only electron beam energy associated with motion perpendicular to the magnetic field axis is available for the beam-wave interaction. Therefore, for an efficient device, a beam with a large ratio of perpendicular to parallel velocities ($v_\perp / v_{||} \equiv \alpha$) is required. Also important is the spread in velocities. Generally, the spread in $v_{||}$ is calculated, since this is a direct indicator of the detuning of the resonance.* Gyrotron oscillators are tolerant of modest velocity spreads, as shown in the cavity calculations discussed below. Beams with values of α between 1 and 2, with $\Delta v_{||} / v_{||}$ of .05 to .2 have been successfully used in other high power gyrotrons.(6)

A magnetron injection gun (MIG) was chosen for the production of the electron beam for the 10 GHz gyrotron. This type of gun is well suited for high power applications, particularly in that it produces an annular beam, which can be located close to the cavity wall, reducing space charge effects. In addition, high current density beams can be generated(6) with the modest velocity spreads.

While all high power gyrotron oscillators reported to date utilized MIG's, most guns have had two anodes, allowing control of the beam parameters by the voltage division between them. It is the authors' experience that the required control can be accomplished by small changes in the magnetic field at

*The resonance condition is $(\omega - k\, v - \Omega_c/\gamma) \simeq \pi$, where ω is the operating frequency (in radians/sec), k, the parallel wave vector, and Ω_c/γ the relativistic cyclotron frequency. $\Delta\alpha$ and $\Delta v_{||}$ are used interchangeably in the manuscript. For a monoergenic beam,

$$\frac{\Delta\alpha}{\langle\alpha\rangle} \simeq \frac{\Delta v_{||}}{\langle v_{||} \rangle} \quad \frac{1}{\langle\alpha\rangle^3} + 1$$

the cathode, and that this electrode is only critical when actually required to realize an electrode configuration[12] or when gating of the beam via the intermediate electrode is desired. For the present gun, which will be large (as shown below), ease of fabrication is an important issue, and the simplicity of a single anode design as shown in Figure 6 is highly attractive. (As will be shown below, the choice of a single anode gun will allow the almost direct use of major subassemblies of an existing electron gun.) Therefore, for the first phase of the gyrotron development a single anode design was pursued.

Basic Parameters

In order to minimize size, a low compression ratio was desired. The minimum acceptable ratio was determined using the adiabatic equation[12]

$$E_c = \gamma_0 \, v_{\perp 0} \, B_{zc}^{3/2} / B_0^{1/2} \cos \phi \qquad (1)$$

which can be recast as

$$E_c = \gamma_0 \, v_{\perp 0} \, B_0 / K^{3/2} \cos \phi$$

where ϕ is the angle between the emitting surface and the axis, B_{zc} and B_0 are the axial components of the magnetic field at the cathode and cavity, respectively, $v_{\perp 0}$ and γ are the perpendicular velocity and relativistic factor of the beam at the cavity (i.e. after compression), E_c is the electric field at the cathode surface, and K is the compression ratio, B_0/B_{cz}

The cathode angle, ϕ, is determined by the equation:

$$\sin \phi = \frac{2\pi \, J_c \, \Delta r \, b \, k}{I}, \qquad (2)$$

where J_c is the current density at the emitter, Δr the spread in guiding center radii at the cavity, b the average guiding center radius, and I the beam current. This expression simply relates the final beam current density

to that of the emitter. Combining the equations we obtain:

$$E_c = \frac{\gamma_0 v_{\perp_0} B_0}{K^{3/2}} \cos\left[\left(\sin^{-1} \frac{2\pi \Delta r\, b\, J\, K}{I}\right)\right]^{-1}. \qquad (3)$$

Using the desired parameters for the electron beam (γ_0 = 1.5 (V ~ 250 kV), v_0 = .6C, B_0 = .44 Tesla, b = 1.73 cm, and I = 200 A), E_c can be plotted as a function of Δr and K. The current density at the cathode, J_c, is taken as the commonly accepted maximum of 10 A/cm^2 for the type B tungsten matrix cathode to be used in the experiment.

E_c is plotted in Figure 4. To avoid electrical breakdown, E_c is normally held at less than 100 kV/cm. Experience has shown that obtaining beams with low velocity spreads are more easily achieved with cathode angles $\gtrsim 45^\circ$. Therefore, from the Figure, a compression ratio of 7 with a cathode angle of 50°, allowing a spread of guiding centers of ~ .2 cm in the cavity, appears to be a good starting point. The spread of .2 cm is still small compared to the larmor diameter of ~ 0.7 cm, and does not cause the beam to intersect more than one peak of the RF field, as can be seen in Figure 5.

The detailed electrode design was carried out using a code originally developed by Herrmannsfeldt.[13] The code calculates electron trajectories within potential boundaries, including the effects of beam space charge, and is fully relativistic. Modeling the temperature limited current mode of the actual gun, the beam current was a specified input. The magnetic field was calculated using a "dummy" coil, with an inner radius of 10 cm, an outer radius of 20 cm, and a length of 50 cm. The actual magnet will differ from this, but will be specified to have the same fields at the cathode and the cavity. This should insure that there are no significant differences in the electron trajectories.

Gun for the $TE_{1,3}$ Cavity

The final design is shown in Figures 6 and 7. An enlargement of the cathode surface is shown in Figure 8. The cathode has an angle of 65^{o}, close to the initial guess, but the required electric field was 45 kV/cm without the beam and 32 kV/cm with the beam, far less than that predicted by adiabatic theory. This is fortunate, in that it allows a much more conservative design (from the standpoint of electrical breakdown) and allows placement of the anode far away from the beam, minimizing the possibility of interception.

The beam parameters at the end of the simulation (i.e. in the cavity) for a current of 200 A are given in Table 1. The average α and $\Delta v_{\perp}/v_{\perp}$ are plotted as a function of beam current in Figure 9. As can be seen, α is approximately 1.5, as desired. The spread in $v_{\perp}$ is 10.7% with a beam current of 200 A. As opposed to other lower power gun designs, the spread drops very slowly with decreasing current. This is apparently caused by the cathode focussing, which has been optimized for high current. This can be seen in Figures 10 and 11, where α of the individual rays used in the code are plotted for the 20 A and 200 A beams. As can be seen, the 20 A case is 'over focussed' - the bottom rays (starting at #1) have been deflected inward by the focus electrode, giving too high an initial perpendicular velocity while the inverse problem is found for the top rays. This focussing is necessary for the high current cases, where the defocussing from the beam space charge would cause the bottom electrons to have too little perpendicular energy, and vice versa, as illustrated in Figures 11 and 12.

The sensitivity to changes in the anode-cathode voltage was examined, as shown in Table 2. Simulations with voltage changes of $\pm$ 2% were made. All of the calculations were for a beam current of 200 amperes. As can be seen, the changes in α are well within the nominal spread in that value, and there is

essentially no change in $\Delta v_{\parallel}$. The modulator for this device is expected to have a voltage variation of at most ± 1%.

Because of the large currents, depression of the beam potential by space charge was expected. This was observed, as illustrated in Figure 13. The potential depression at the nominal operating current of 150 A is 16 kV (7%) with a 5 kV spread in the beam energy. This 2% spread should not effect the operation. Also indicated in the figure is the limiting current as predicted by Ganguly and Chu.[14] As can be seen, the analytical theory predicts a limiting current less then the current calculated by the code.

$TE_{1,4}$ Gun

A gun to produce a beam for the $TE_{1,4}$ cavity was also designed. The principal difference is that the beam is closer to the cavity wall, reducing the space charge depression. The results of the simulation are shown in Figures 14-17 and Table 1. As expected, the space charge depression is lower than that found in the $TE_{1,3}$ gun. This reduction in space charge allows propagation of reasonable quality beams with currents to 300 amperes. The compression ratio required to realize the gun was substantially lower than that for the $TE_{1,3}$ gun, 5.8 vs 8. The lower compression ratio in conjunction with reduced space charge resulted in a much lower value of $\Delta v_{\parallel}/v_{\parallel}$ - 6.5% at 300 amperes. The spread at 200 amperes was 6.8%, the slight rise due to over focussing. This could probably be improved, since, as shown in Figure 17, the plot of α vs ray number is essentially linear, and could be "tilted" with better (reduced) focussing. This gun then may well be useful for a gyroklystron, where velocity spread is much more detrimental to the efficiency, and mode competition may be less of a factor.

Cavity Design

$TE_{1,3}$ Cavity Analysis

A cavity with a profile as shown in Figure 18 was chosen for the initial calculations. The slight taper at the input has been shown in previous designs to increase the efficiency[15] and reduce mode conversion at the input step. The taper at the output was chosen to achieve the required Q, and may produce an unacceptable amount of conversion to other $TE_{1,n}$ modes. This problem will be examined in later calculations, and can be corrected by use of either a compound taper or a shallow iris.

For calculation of the efficiency and starting currents, a code developed by Fliflet[16] was used. In this code, the efficiency is calculated by integrating the electrons through their orbits in an RF field calculated for the cavity without the beam. The calculations are for a standing mode (i.e. one with azimuthal variation given by $\cos(m\theta)$, as is required to produce a linearly polarized output.

Consistent with calculations of the beam characteristics made above, the beam voltage was taken as 218 kV, with a ratio of perpendicular to parallel beam velocities ($\equiv \alpha$) of 1.5. Calculations were made with both zero and 11% spreads in $v_{||}$. The beam energy was assumed to be monoenergetic. The average beam radius was 1.7 cm.

Results of the calculations are shown in Figures 19, 20 and 21. With zero spread in $v_{||}$ a maximum efficiency of 33% is indicated, and 10 MW should be produced with a beam current of 140 Amperes. With $\Delta v_{||}/v_{||} = 11\%$, the efficiency drops to 31%, and 148 Amperes are required for 10 MW output. With 250 Amperes, the maximum planned for the electron gun, approximately 14 MW should be produced with an efficiency of 27%, even with the effects of velocity spread.

The starting currents were calculated with the same code. The modes considered were the $TE_{3,2}$, $TE_{7,1}$ and $TE_{0,2}$. The results are shown in Figure 22. Assuming that the mode with the lowest starting current will predominate for any given magnetic field, the $TE_{1,3}$ mode will clearly suffer from competition from the $TE_{3,2}$ mode. The effect of this can be seen in Figure 23, were the output power in the $TE_{1,3}$ mode has been plotted with the assumption that operation with magnetic fields less than .45 Tesla is impossible. As can be seen, the effect is not severe, with only about 10 percent of the efficiency lost. An additional (approximately) 5% will be lost due to velocity spread. Ten MW now requires about 158 Amps, well within the allowed range of current.

However, these calculations are only approximate indicators of mode competition, and suppression of unwanted modes may be necessary. Calculations based on a two dimensional, single mode model[17] indicate that such suppression is possible. With slots in the cavity wall, the unwanted modes are predicted to have Q factors due to the slots which are substantially less than the Q produced by the the normal output, while the desired mode should have a "slot Q" much higher than the output Q. This is shown in Figure 24. However, cold tests indicate that the simple insertion of slots in a cavity is not effective in selectively reducing the total Q, probably because the introduction of the slots causes considerable mode conversion. This may have been due to end effects in the actual cavity or inherent coupling between modes that are not modeled by the explicitly single mode model. Clearly, further research is required on this subject.

$TE_{1,4}$ Cavity

Similar calculations were made for the $TE_{1,4}$ cavity with the average beam radius at 3.2 cm. The cavity profile is shown in Figure 25. Again reflecting

the results of the beam calculations, the average beam energy was taken to be 225 keV, and α equal to 1.5. The energy is higher in this case because the beam is located closer to the cavity wall, reducing the space charge depression.

The results are shown in Figures 26 and 27. As can be seen, the results are similar to those obtained with the $TE_{1,3}$ cavity. A slightly higher peak efficiency was obtained, due to the fact that a longer cavity could be used to produce the same power with the larger cavity. However, the results of the starting current calculations (Figure 28) are quite different. There are now 3 competing or nearly competing modes, with the $TE_{6,2}$ mode being almost degenerate with the desired mode. Because the $TE_{6,2}$ mode has a broader peak in the plot of field versus radius, it is probable that this mode would always be preferentially excited. Thus it would be definitely necessary to modify the cavity to suppress this mode.

Further research on this problem is being persued, but it is clear that efficient operation of the $TE_{1,4}$ mode will require substantially more effort that the $TE_{1,3}$ mode.

Collector

The most obvious collector is one which also serves as the output guide, and is thus a smooth wall tube. For a reasonably large radius and thickness tube, the heat diffusion problem can be modeled as one dimensional and semi-infinite. The solution for the temperature rise in the medium is by given approximately by[18]

$$\Delta T = \frac{2F_0}{K}\left(\frac{\kappa t}{\pi}\right)^{1/2} e^{-x^2/4\kappa t} - \frac{x}{2}\,\mathrm{erfc}\left(\frac{x}{2\sqrt{\kappa t}}\right). \tag{4}$$

At the surface ($x = 0$) ΔT is

$$\frac{2F_0}{K}\left(\frac{\kappa t}{\pi}\right)^{1/2}. \tag{5}$$

F_0 is the flux of heat per unit time, K is the thermal conductivity, κ the diffusivity, x the spatial dimension normal to the surface and t, time. (All units are c.g.s.) For copper at room temperature, K = .93 cal/(sec) (cm) (^oC) and $\kappa = 1.14$ cm^2/sec. The surface temperature rise will then be

$$\Delta T \cong 1.3\, F_0\, t^{1/2}. \tag{6}$$

A temperature rise of 100^o is generally considered to be the maximum tolerable without there being concern for damage due to repetitive pulsing. Then,

$$F_0 \lesssim \frac{100}{1.3\, t^{1/2}}. \tag{7}$$

For a 100 microsecond pulse,

$$F_0 < 7.7 \cdot 10^3 \text{ Cal/sec cm}^2$$

or

$$F_0 \lesssim 30.9 \text{ kW/cm}^2.$$

For a 50 MW beam, an area of 1618 cm^2 is required.

The pentration depth, x_0 is of interest, in order to check the initial assumption of a semi-infinite medium. From equation (4), it is

$$x_0 \cong 2 (\kappa t)^{1/2},$$

equal to .02 cm. Clearly the assumption is valid for practical wall thicknesses. It is of note that the thermal diffusion length is only twice the electron energy deposition length.[19] This fact should make the above calculation somewhat conservative.

The beam from the $TE_{1,3}$ electron gun was integrated through to a 'collector', as shown in Figure 29. The collector diameter was chosen rather arbitrarily as 20 cm. (The diameter is 6-7 wavelengths. Collector diameters of 12.7 wavelengths have been shown to function as output waveguides without unacceptable mode conversion.)[6] With this collector, the beam is spread over roughly 1000 cm^2.

To spread the beam over a larger surface, either the collector can be made larger in diameter, or the magnetic field modified so that the beam will impact over a longer length. The longer length is attractive because a large diameter will make it difficult to magnetically deflect "errant" electrons away from the window. In fact, reducing the diameter to 6" would require a length of 34 cm (13") - a very reasonable length. Increase of the length will require addition of magnetic fields of on the order of 100 Gauss.

Output Window

Since the average power will be low (< 10 kW), a single disk window, either edge cooled by water or face cooled by air can be used. Three parameters are of interest for the window: the stress caused by the atmospheric pressure, the power deposited in the window, and the peak electric field. 'If

the result of the second calculation indicated a significant deposition, the stress due to thermal variations would have to be calculated.)

The maximum stress on a simply supported disk is given as[22]

$$S = 3/8 \frac{wr^2}{t^2} (3 + m) \quad \text{(p.s.i.)}$$

where w is the distributed load in pounds per square inch, r is the radius in inches, and t is the thickness. m is Poisson's ratio. The maximum deflection is (in inches) given by

$$\Delta = \frac{2}{3} \frac{wr^4}{Et^3}$$

where E is Young's modulus. For a window with thickness, t, greater than one tenth the wavelength in the dielectric, λ_w, to avoid reflection,

$$t = \frac{n\lambda_w}{2} \qquad n = 1,2,3, \ldots$$

A table of the stress and strain for windows of common grades of Alumina and Beryllia are given in Table 3. The tensile and flexural strengths are given in Table 4. As can be seen, a window of thickness equal to λ_w would be satisfactory for all materials even with a 30 cm (12") diameter and $\lambda_w / 2$ would be satisfactory for a 6" window. Windows with similar thicknesses have been used successfully at higher frequencies in the authors' laboratory.

The loss in the windows is given by

$$P_L = P_0 (1 - e^{-2\alpha z})$$

where

$$\alpha = \frac{\pi}{\lambda_w} \frac{\varepsilon''}{\varepsilon'} .$$

The loss tangent, $\sim \frac{\varepsilon''}{\varepsilon'}$, at 10 GHz, is equal to $\sim 4 \cdot 10^{-5}$ for Alumina and $1\ 10^{-4}$ for BeO.

For alumina, the loss is $\sim$ 2.3W for $t = \lambda_w$; for BeO, $\sim$ 4.8 W For the size windows being considered, the losses can be handled easily.

The peak electric field for $TE_{1,n}$ modes on center is given as by

$$E_{rp} = (Z_{TE}\, W_T)^{1/2} \left(\pi\, a^2\, J_n^2\, (X) \left(1 - \frac{1}{X^2} \right) \right)^{-1/2}$$

where Z_{TE} is the impedance of the (TE) wave, W_T is the total power, and X is a root of J_n. For n = 3, X = 8.536 and $Z_{TE} \cong 400$ ohms, $E_{rp} \simeq 18.42$ kV/cm for a = 7.6 cm and 9.3 kV/cm for a = 15 cm.

It is useful to compare this number to the field at the window of a 35 MW, S band klystron as used at the Stanford Linear Accelerator. With standard S band rectangular guide, (8.6 cm x 4.3 cm), a peak field of approximately 27 kV/cm is found.

Although the field of the gyrotron is substantially less than that of the klystrons, spot heating due to thin films applied to suppress multipactor may be a problem, particularly since the pulse length is 100 μs, as opposed to 2 μs for the S.L.A.C. klystron. Thus, while the basic window design seems straightforward, further consideration must be given to this element.

Mode Converter

Converters for transformation of $TE_{n,m}$ to $TE_{n,p}$ modes have been successfully designed and tested at higher frequencies.[9] These converters are of the 'rippled wall' type, and have the geometry shown in Figure 31. The conversion is accomplished entirely within waveguide. For the present case, conversion from the $TE_{1,3}$ to the $TE_{1,1}$ mode is desired. Design of such a converter should be straightforward. Scaling from previous designs,[9] over 95% conversion is expected in a device of length of 1M - 2M.

Gun Fabrication

The electron gun is the highest technology element of the gyrotron. In order to reduce the risk and long lead times involved with a totally new gun design, an attempt was made to identify and utilize portions of an electron gun design which had the same basic parameters of voltage and current. Such a gun appears to be that used with the SLAC 50 MW klystron, currently beginning production. This gun is designed to operate at 300 kV, with a 2 μs pulse width. Degrading the voltage to 250 kV and increasing the anode radius should insure operation at 100 μs. (The peak electric field, which occurs near the front top corner of the cathode, is 137 kV/cm. This is significantly lower than the 200 kV/cm normally allowed for pulsed operation.) A schematic of the gun is shown in Figure 33. Of interest for the gyrotron is the cathode support structure and base and the high voltage insulator. These can be used for the gyrotron gun by monitoring the cathode and anode as shown in Figure 34. This should produce a reliable gun with minimum expense and time.

Conclusion

A design for a 10 MW, 10 GHz gyrotron with a maximum pulse length of 100 μs has been described. The design appears without major risks. The design is summarized in Table 5, and is shown schematically in Figure 32. Two cavities and their respective electron guns have been investigated. The $TE_{1,4}$ cavity is more satisfactory when it is examined without regard for mode competition, but is predicted to suffer strongly from this problem. The $TE_{1,3}$ cavity may operate satisfactory with suppression of unwanted modes, although prudence indicates that suppression methods be prepared. The gyrotron using this mode should have good efficiency (~ 28%) and a margin of safety in power of over 40%. The gun should produce a beam with an acceptable velocity spread, and its operation is predicted to be stable to changes of current and voltage. Therefore, the $TE_{1,3}$ mode will be used initially as the operating mode.

There are clearly further calculations needed, particularly in the design of the cavity. Mode conversion in the input and output tapers must be addressed, although previous experience indicates that with careful design, a mode of at least 90% purity can be realized. Clearly the mode converter must be designed. Finally, the output window must be carefully studied, since this element is often a focal point for failure in high power tubes.

Acknowledgments

The authors would like to thank K. Gardner for running of the Hermannsfeldt Code, R. Lee for preparation of that code for our problem, R. Bosenburg for technical advice, and Drs. A. Fliflet and J. Lebacqz for useful discussions. The work was supported by the U.S. Army.

TABLE 1

Beam Parameters for the Electron Guns

	$TE_{1,3}$ Gun	$TE_{1,4}$ Gun
Accelerating Voltage (kV)	240 kV	240 kV
Current (A)	200	200
$v_\perp / v_{\|\|}$	1.5	1.58
$\Delta (v_\perp / v_{\|\|})$ (%)	15.8	9.60
$\Delta v_{\|\|}$ (%)	11.0	6.77
Potential Depression (kV)	22	15

TABLE 2

Sensitivity of Beam Parameters

to the Anode-Cathode Voltage

the $TE_{1,3}$ Gun

V_{a-k}	$\langle\alpha\rangle$	$\Delta\alpha/\langle\alpha\rangle$	$\Delta v / \langle v \rangle$
-244.8 kV (+2%)	1.62	.148	.106
-240 kV	1.55	.158	.110
-235.2 kV (-2%)	1.45	.154	.102

TABLE 3

Stress and Strain for Alumina and Beryllia Windows

		Stress on Center (psi)		Strain on Center (inches)	
r	t	Alumina	BeO	Alumnia	BeO
3.0 (7.6 cm)	λ/2	4,650	2,900	$2.4\ 10^{-3}$	$1.2\ 10^{-3}$
	λ	1,160	725	3.0^{-4}	$1.5\ 10^{-4}$
	3/2 λ	517	325	$9.1\ 10^{-5}$	$4.7\ 10^{-5}$
5.9 (15 cm)	λ/2	18,000	11,300	$3.7\ 10^{-2}$	$1.8\ 10^{-2}$
	λ	4,500	2,800	$4.6\ 10^{-3}$	$2.3\ 10^{-3}$
	3/2 λ	2,000	1,250	$1.4\ 10^{-3}$	$6.9\ 10^{-4}$

	Alumina		BeO	
λ/2	.19"	(.48 cm)	.24 "	(.61 cm)
λ	.37"	(.94 cm)	.47 "	(1.19 cm)
3 λ/2	.56"	(1.42 cm)	.71 "	(1.80 cm)

E	$\sim 50.10^6$	50.10^6
Poisson's Ratio	.21	.26

TABLE 4

Tensile and Flexural Strengths of
Window Materials at 25°C

	Alumina	BeO
Tensile Strength (psi)	$20\text{-}35 \cdot 10^3$	$20 \cdot 10^3$
Flexural Strength (psi)	$45 \cdot 10^3$	$35 \cdot 10^3$

TABLE 5

Summary of Gyrotron Designs

	$TE_{1,3}$	$TE_{1,4}$
Frequency	10 GHz	10 GHz
Gun Voltage	240 kV	240 kV
Beam Current Nominal	158	142
Maximum	250	250
Output Efficiency		
at nominal current	31%*	28%*
at maximum current	33%	30%
Output Power		
at nominal current	10 MW	10 MW
at maximum current	14.7 MW	16.9 MW
Polarization	linear	
Pulse Length	1 μs - 100 μs	
Duty Cycle	$\leq 10^{-3}$	
Maximum Average Power	10 kW	

* Includes the effects of mode competition, potential depression, and velocity spread.

** Includes the effects of potential depression. Velocity spread is expected to be unimportant. Mode competition will be severe without suppression.

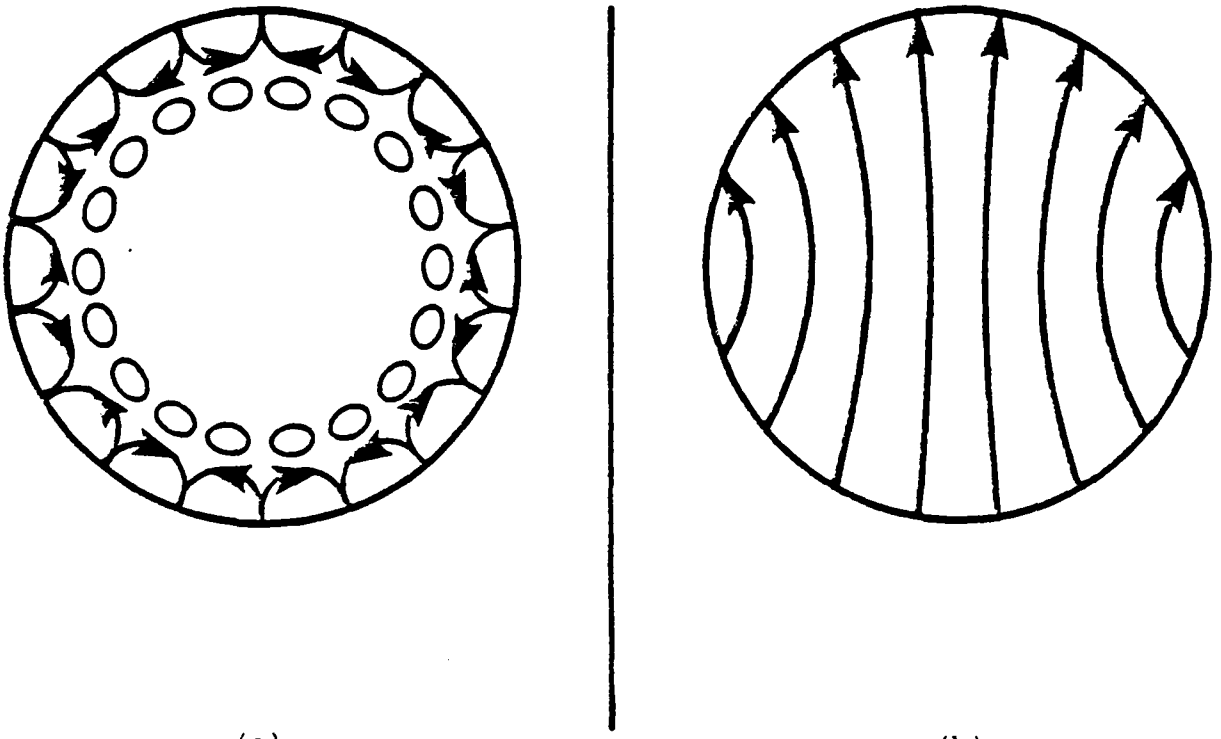

(a) (b)

Fig. 1. (a) Electric field lines of a $TE_{m,2}$ mode in a circular cavity. (b) Same, of a $TE_{1,1}$ cavity.

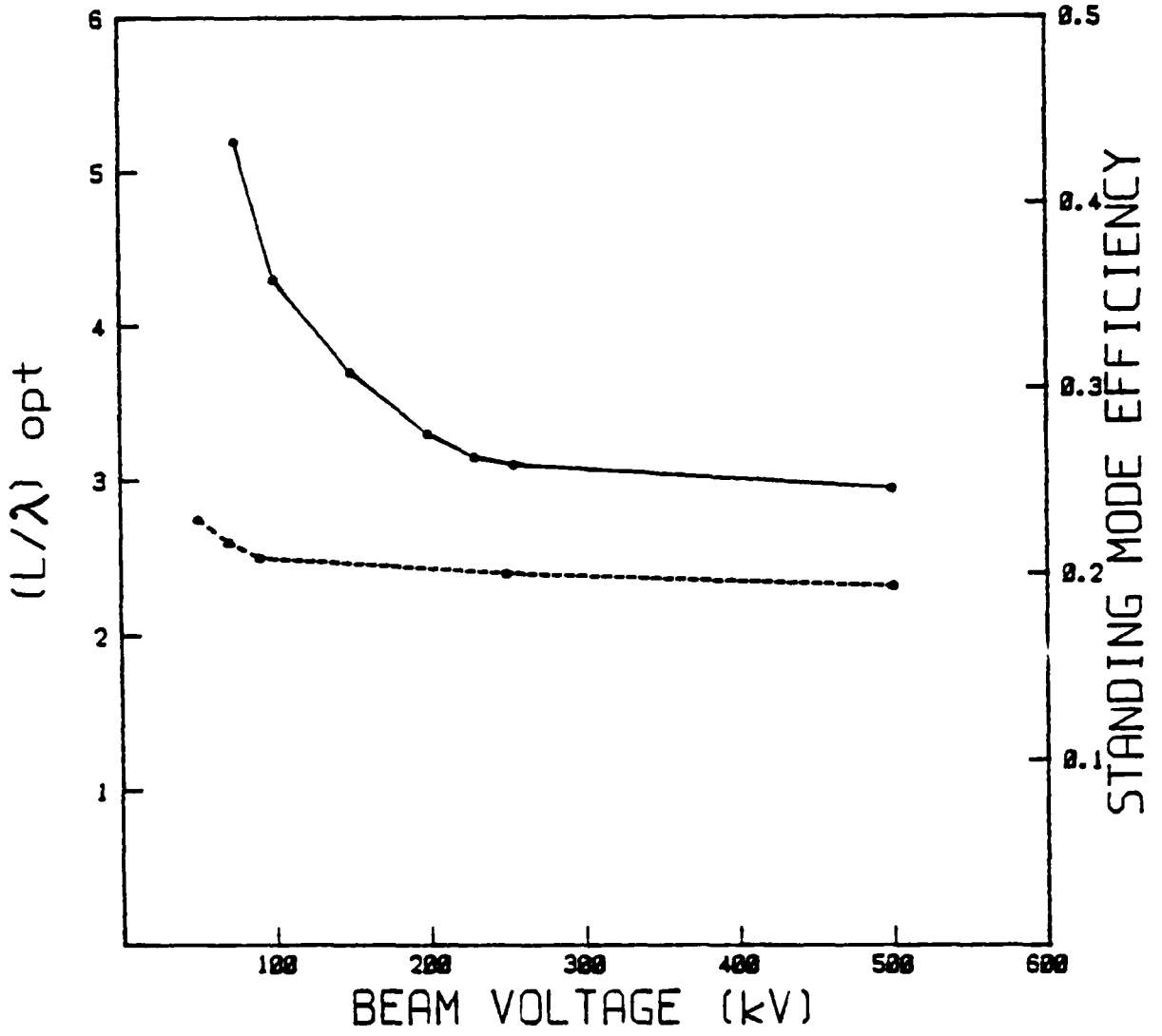

Fig. 2. Plot of cavity lengths which give optimum efficiency as a function of beam voltage for $\alpha = 1.5$.

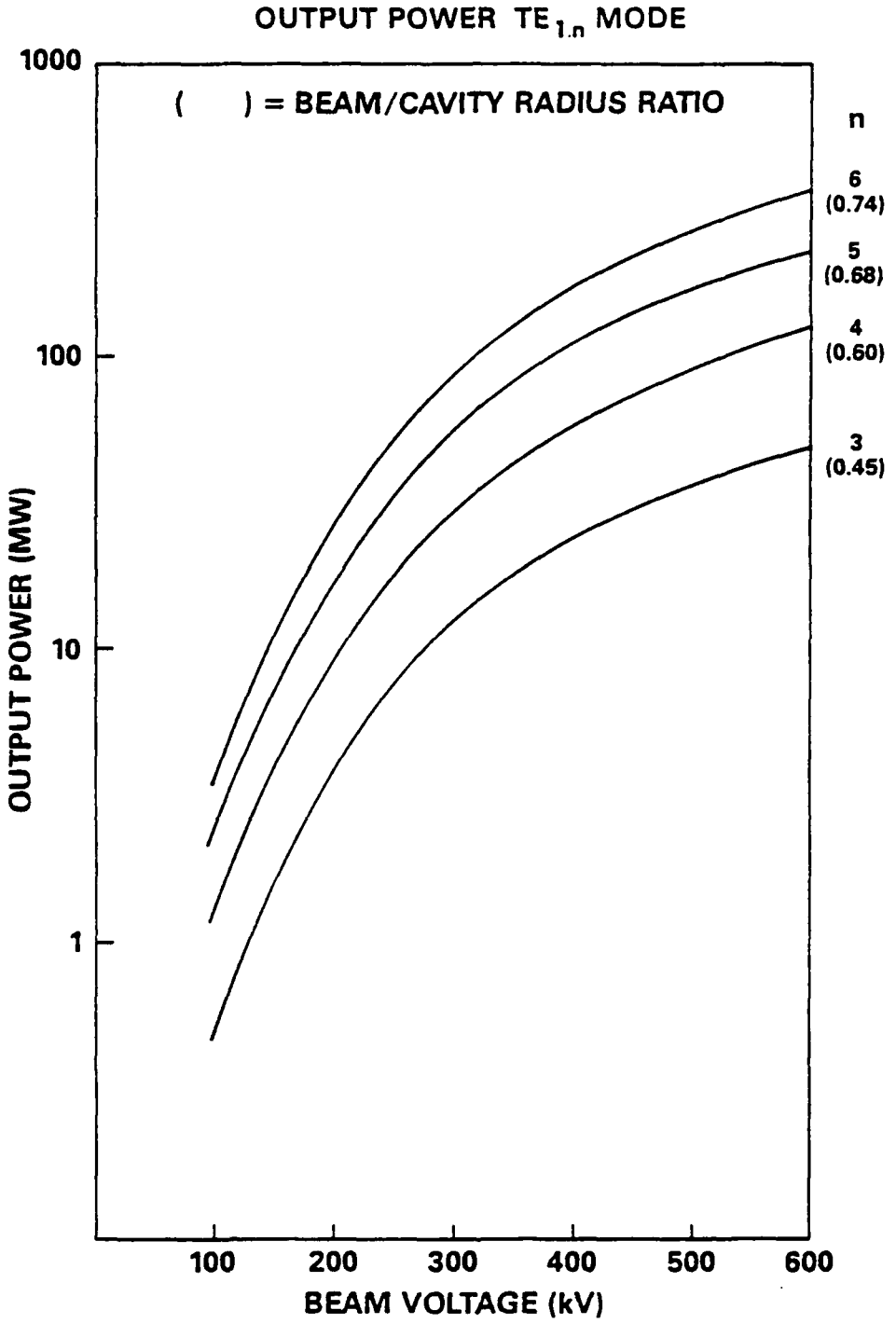

Fig. 3. Plot of output power verses beam voltage for several $TE_{1,n}$ modes. Anα of 1.5 and Q equal to twice the diffraction Q was used. The calculations were performed by integrating the beam electron through an RF field with an assumed axial profile of a half-sinusoid, with optimum length.

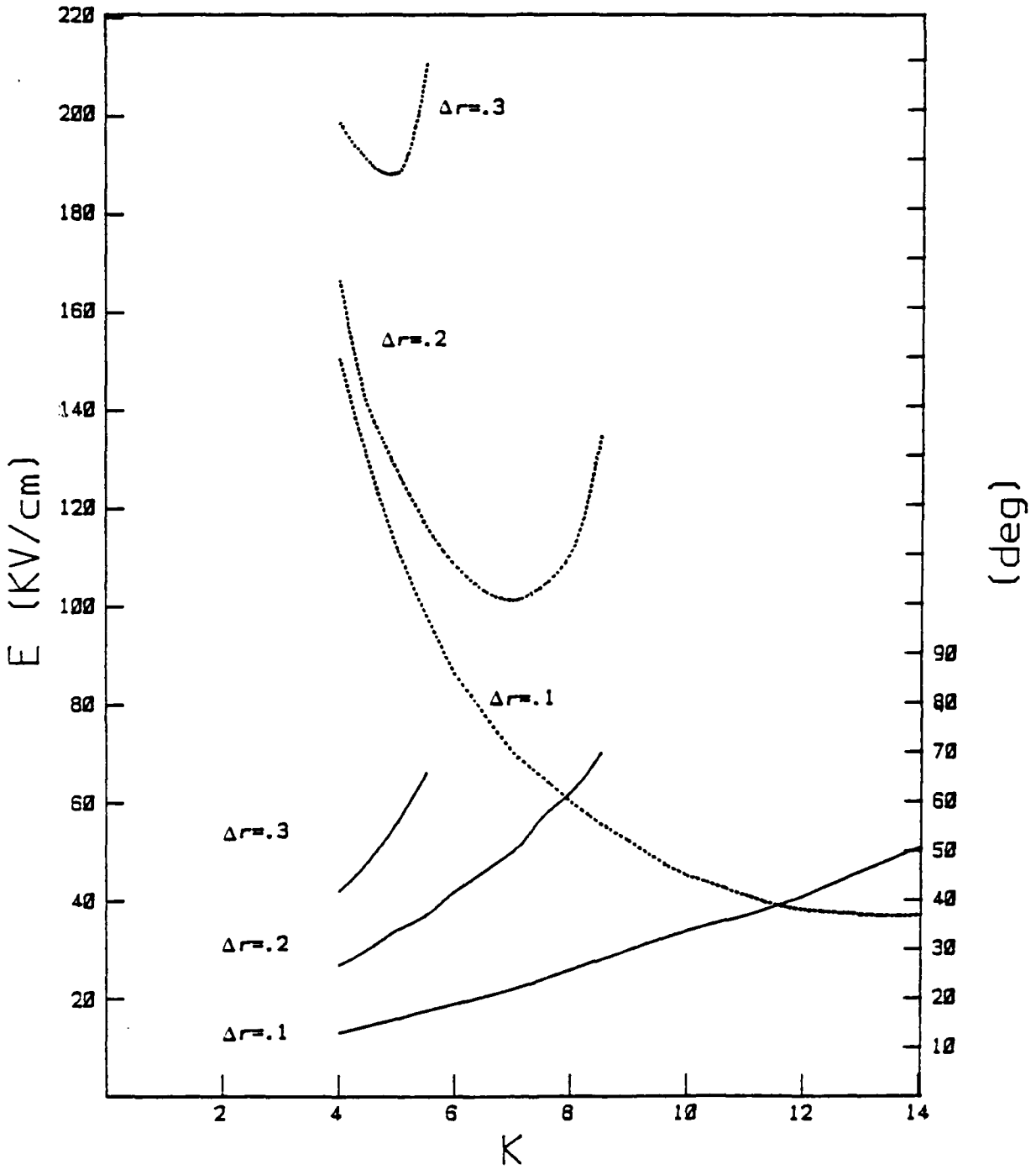

Fig. 4. Plot of the cathode electric field required for production of a beam with $\alpha = 1.5$ with an anode cathode voltage of 250 kV (solid lines) and the angle of the cathode surface with respect to the axis (dashed lines), as a function of the compression ration k and the spread in the guiding center radius.

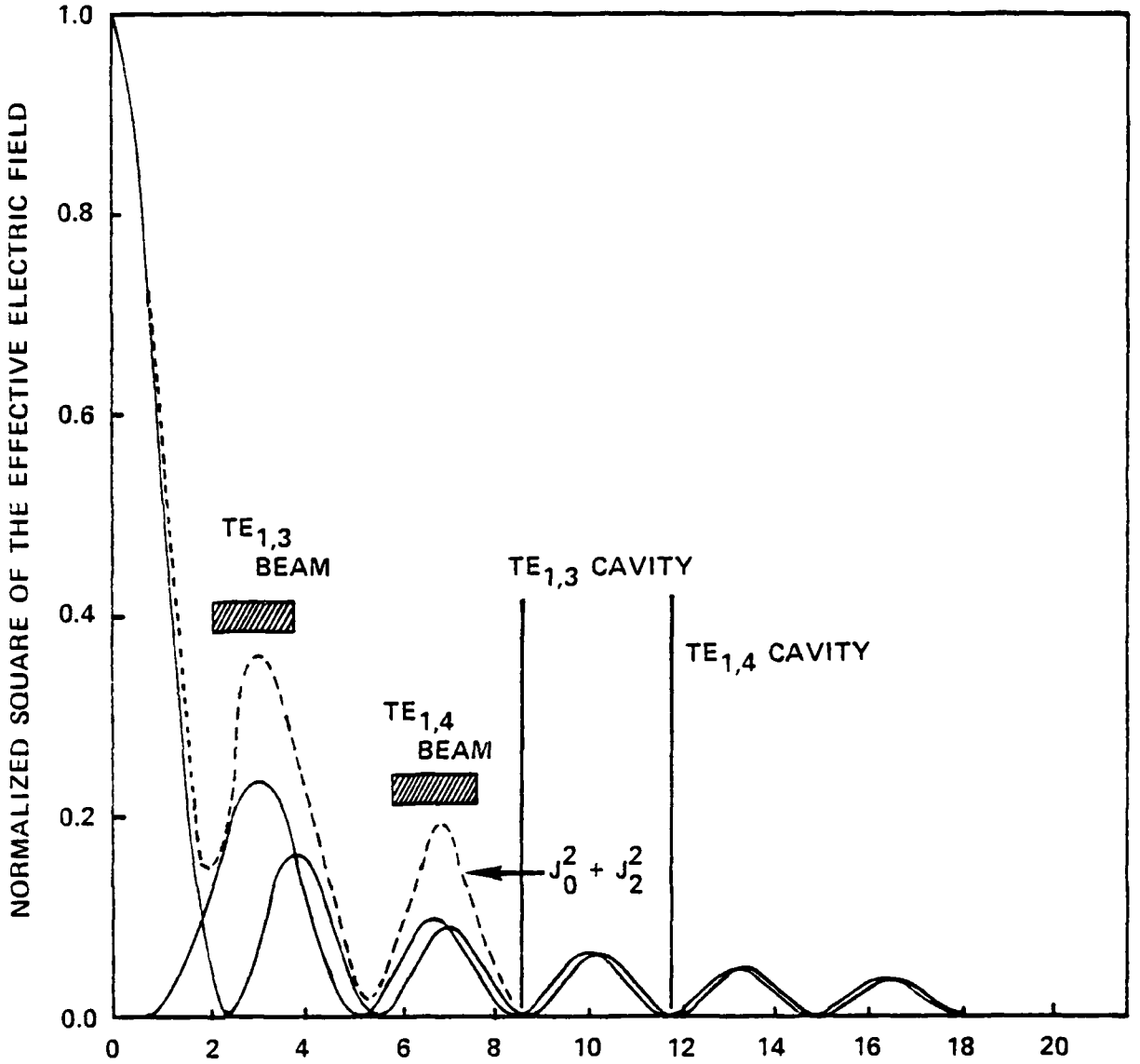

Fig. 5. Plot of the beam radial extent superimposed on a plot of the normalized effective RF electric field in the $TE_{1,3}$ and $TE_{1,4}$ cavities.

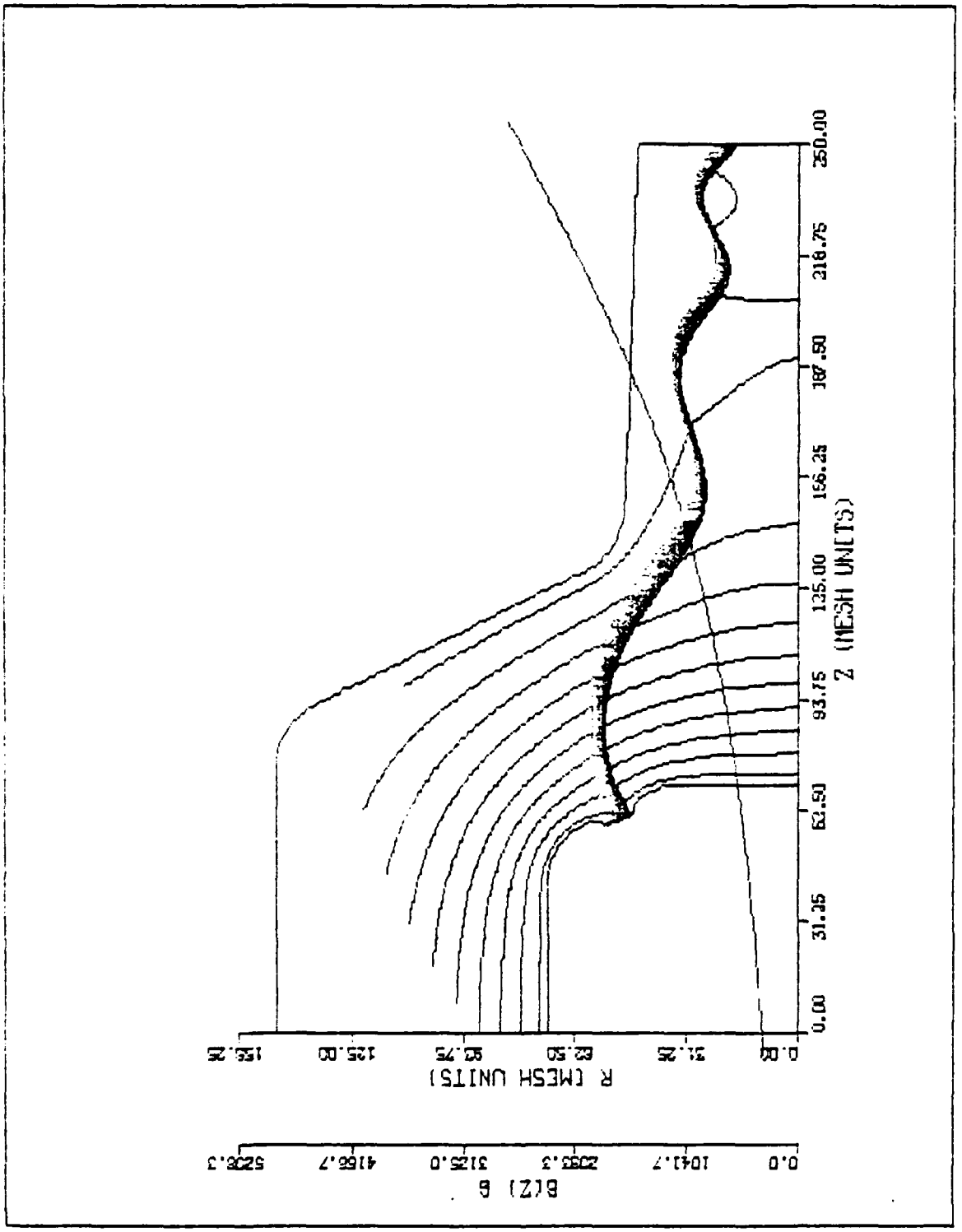

Fig. 6. Schematic and beam trajectories of the electron gun for the $TE_{1,3}$ cavity. The A-K voltage is 240 kV; the current 200 A. The mesh size is 1 mm.

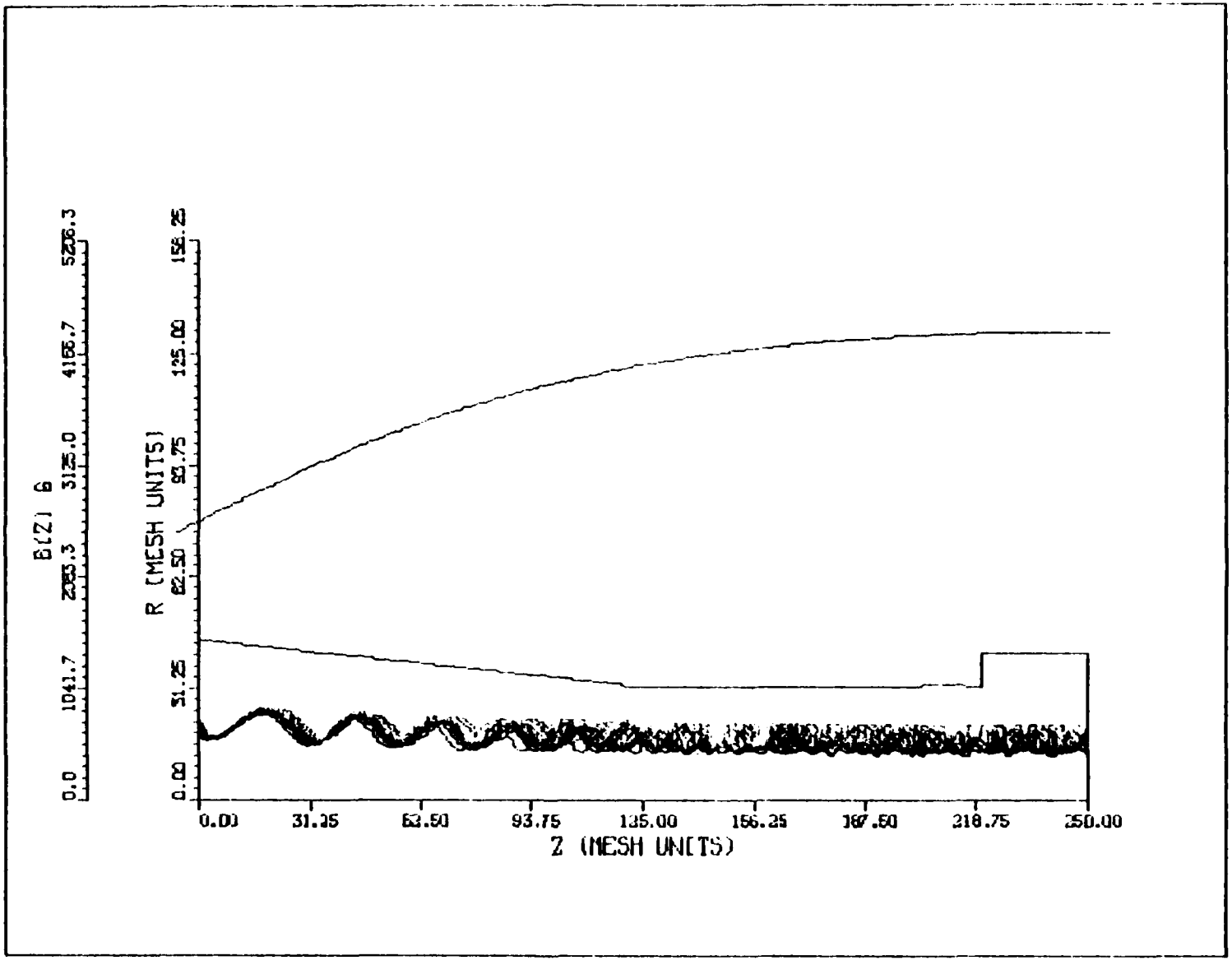

Fig. 7. Continuation of the beam trajectories of Figure 17, shown to the cavity.

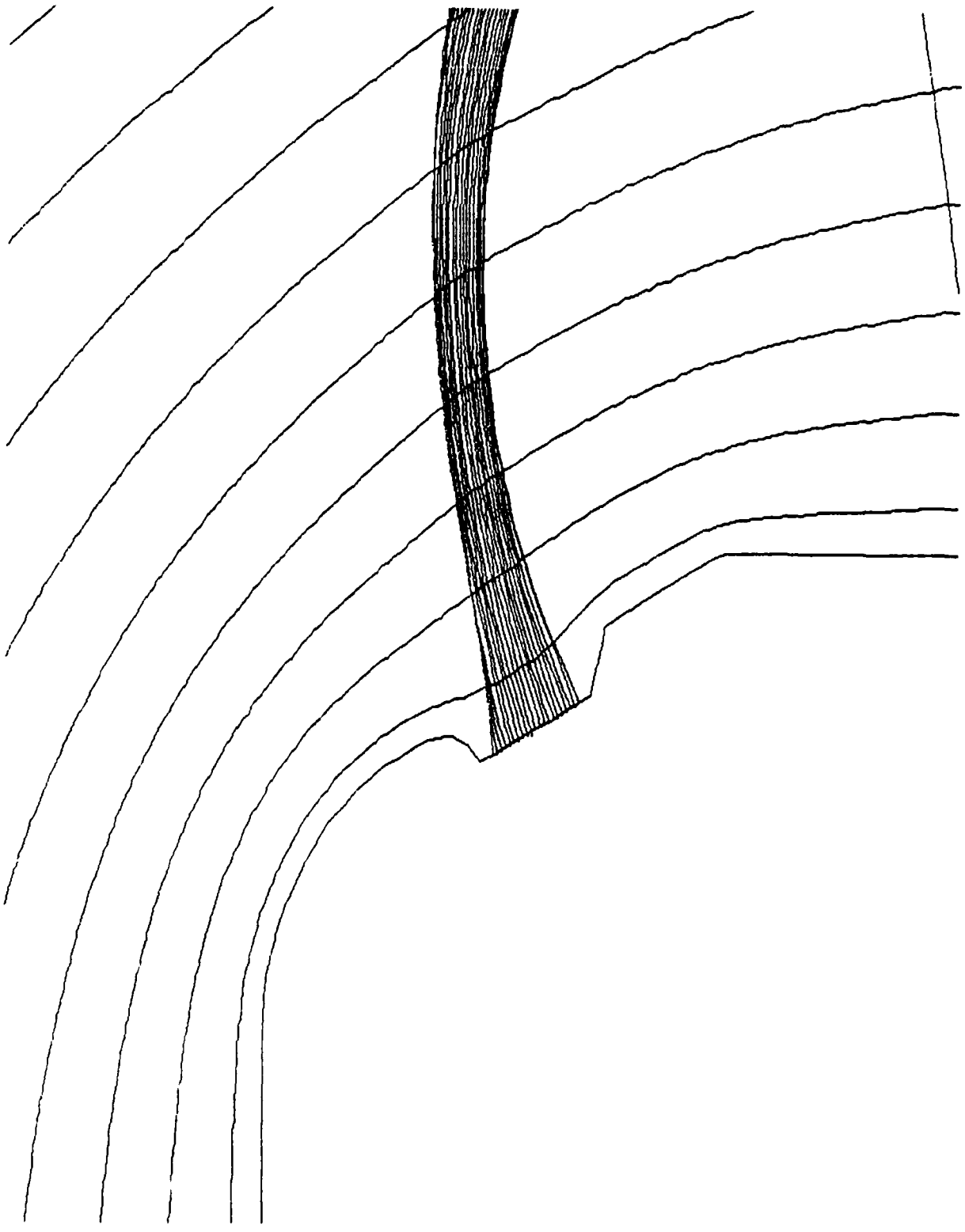

Fig. 8. Enlargement of the region near the cathode of Figure 17.

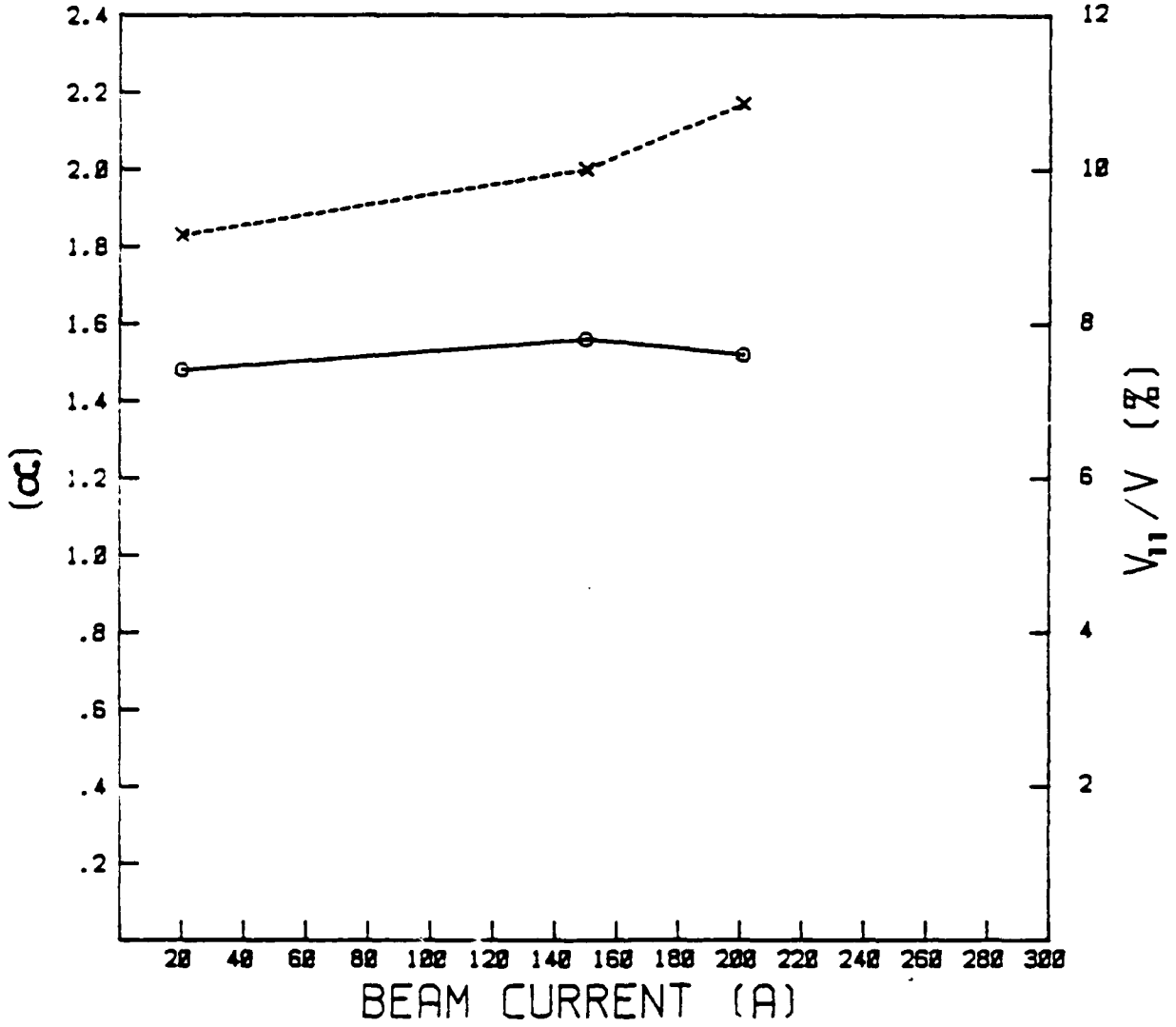

Fig. 9. Plot of the average α (solid line) and Δv /v (dashed line) as a function of beam current, for the $TE_{1,3}$ electron gun. The accelerating voltage was 240 kV.

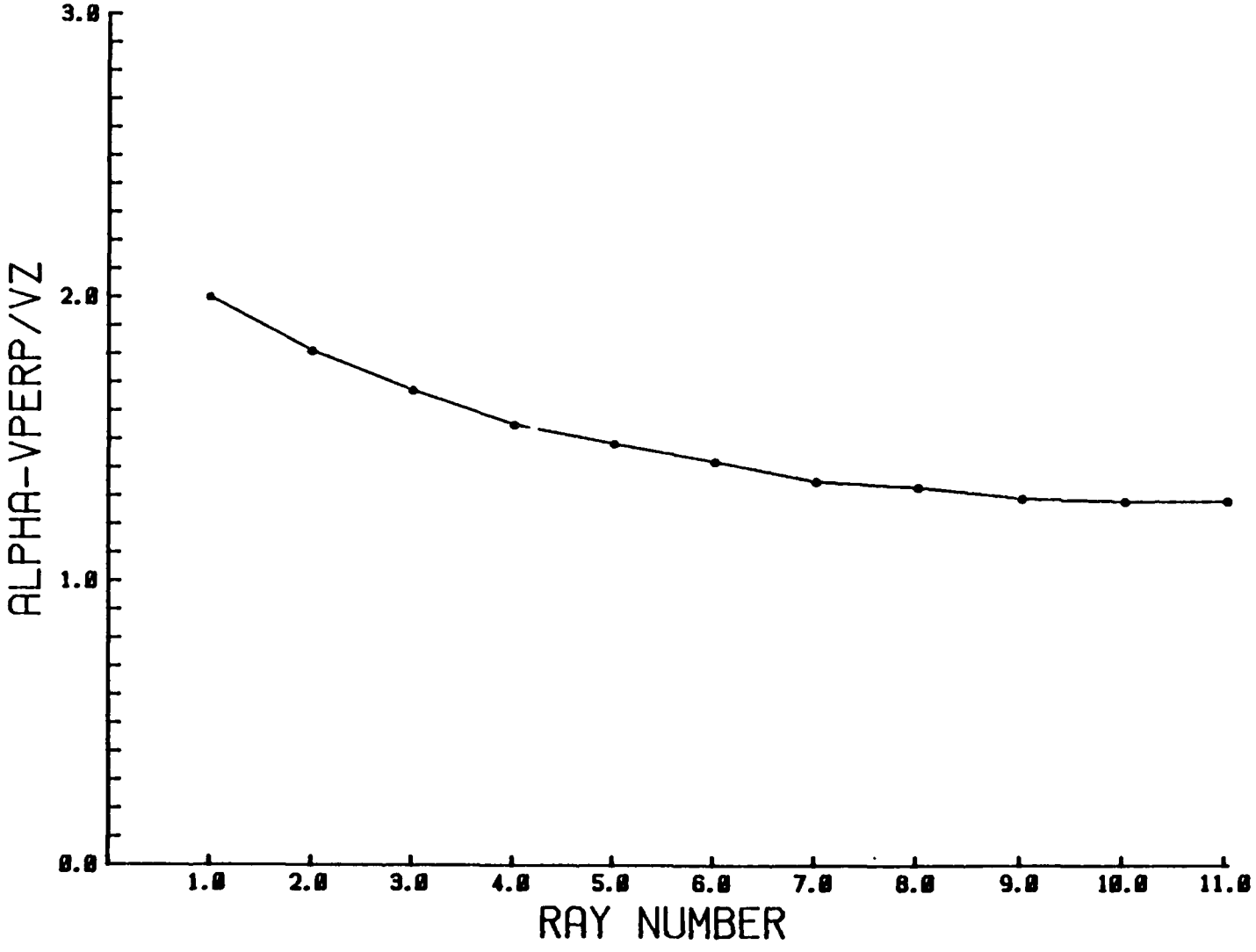

Fig. 10. Plot of the values of α for the individual electron trajectories for the $TE_{1,3}$ gun, calculated at the cavity, for a beam current of 20 A. Trajectory #1 originates at the bottom of the emitting surface.

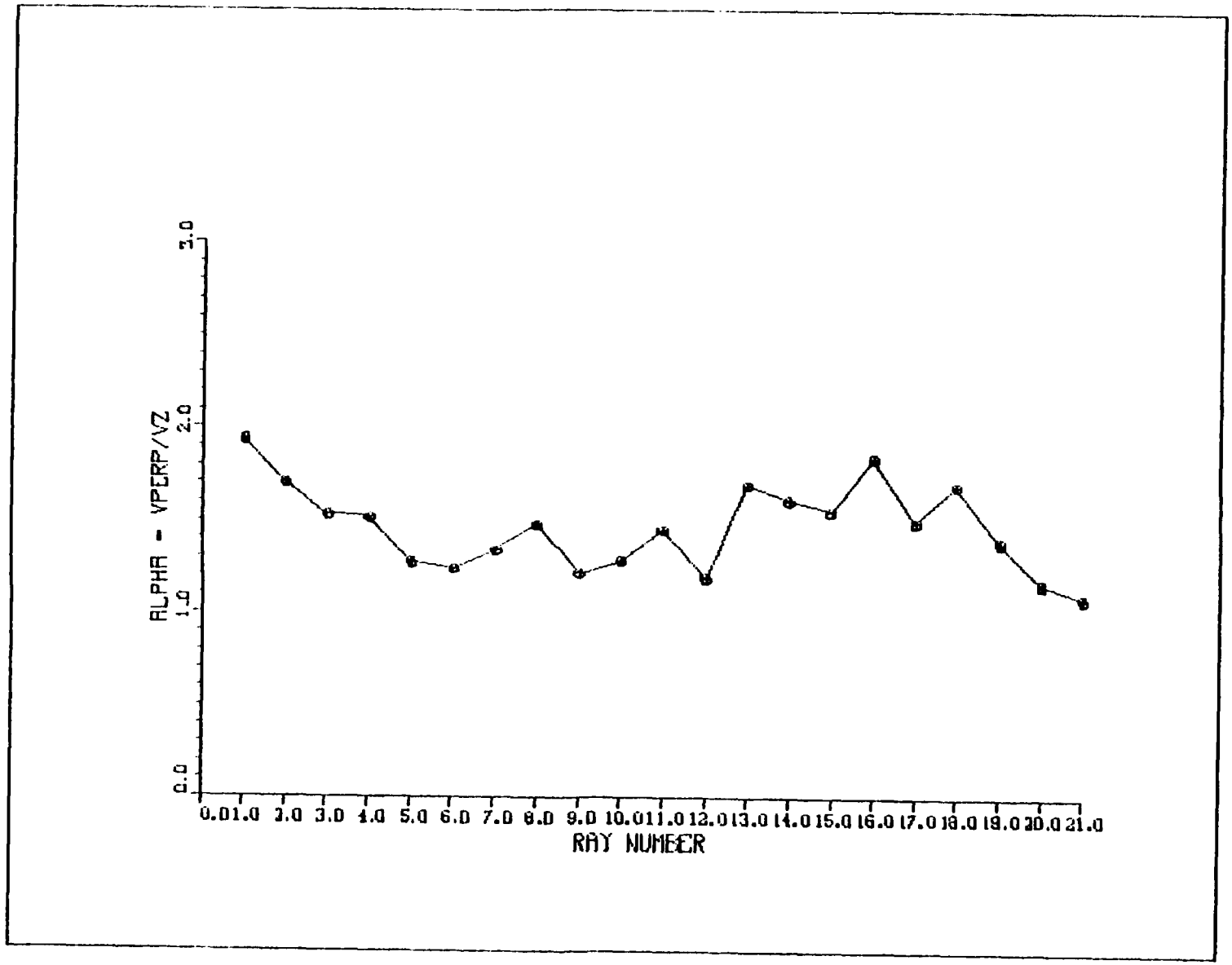

Fig. 11. As Figure 21, but for a beam of 200 A.

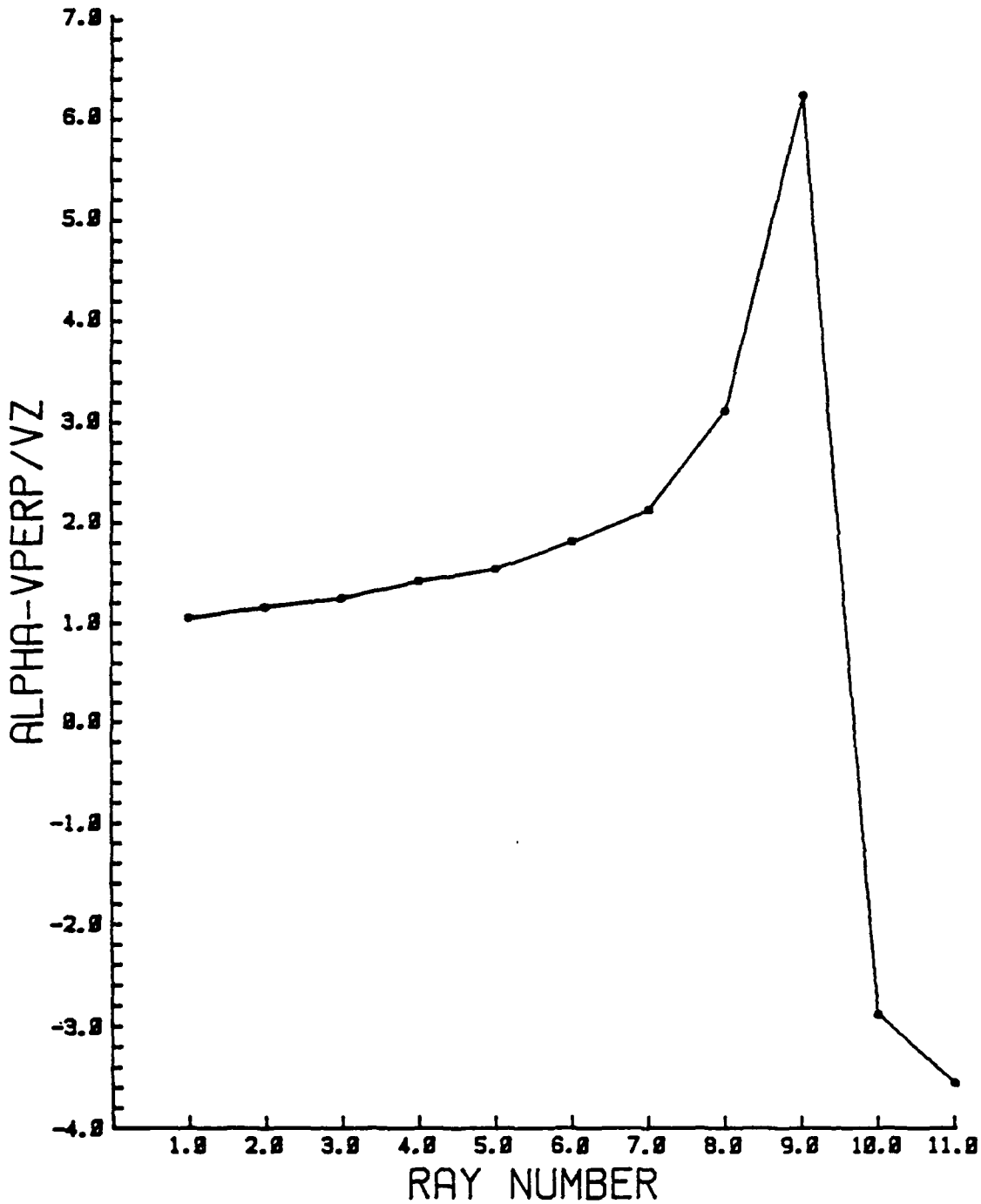

Fig. 12. As Figure 21, but for a 200 A beam generated by a cathode without focussing.

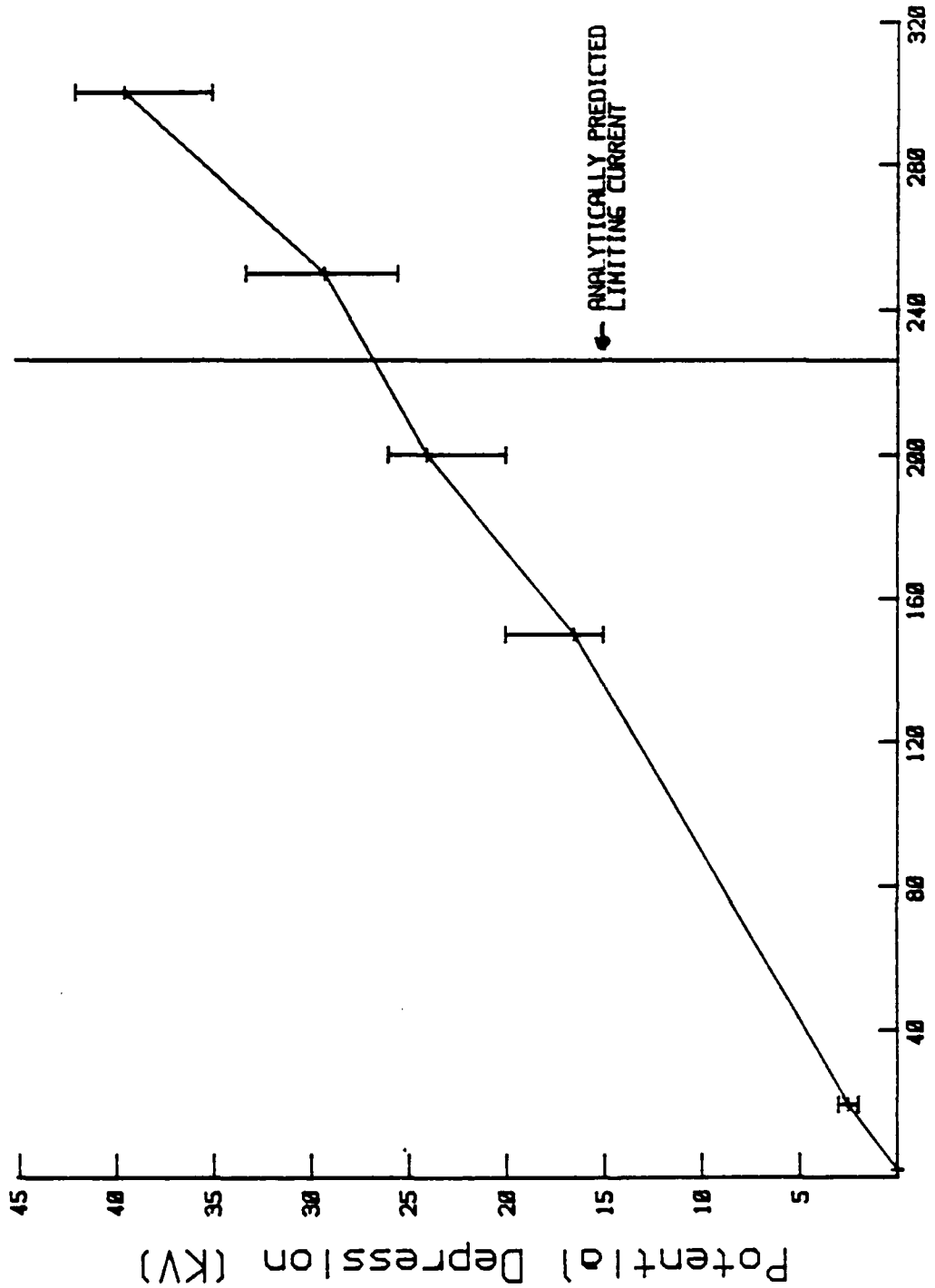

Fig. 13. Plot of the potential depression of the beam from the $TE_{1,3}$ electron gun, as a function of beam current. The symbol x indicates the average depression, the I indicates the spread in voltage across the beam.

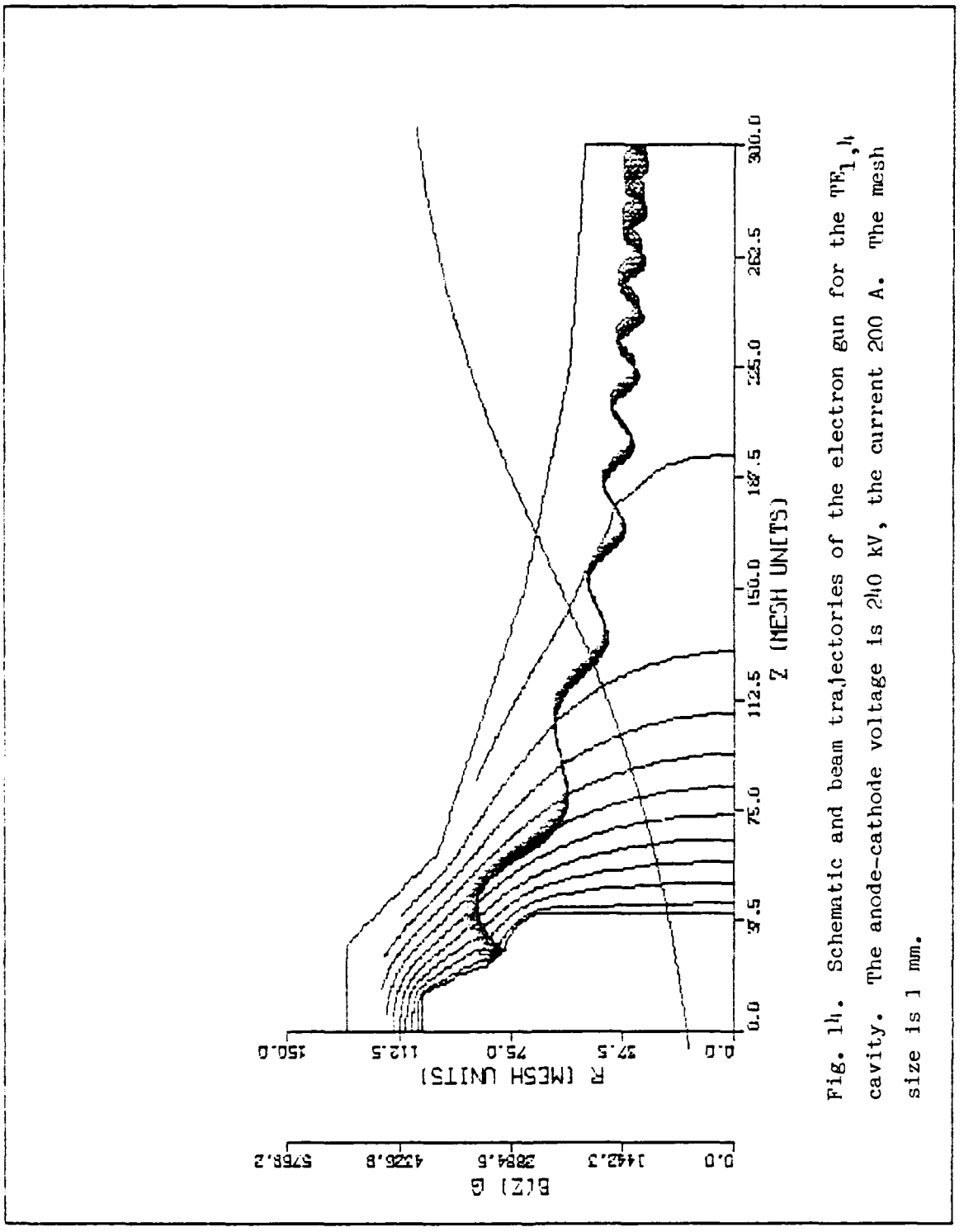

Fig. 14. Schematic and beam trajectories of the electron gun for the $TE_{1,1}$ cavity. The anode-cathode voltage is 240 kV, the current 200 A. The mesh size is 1 mm.

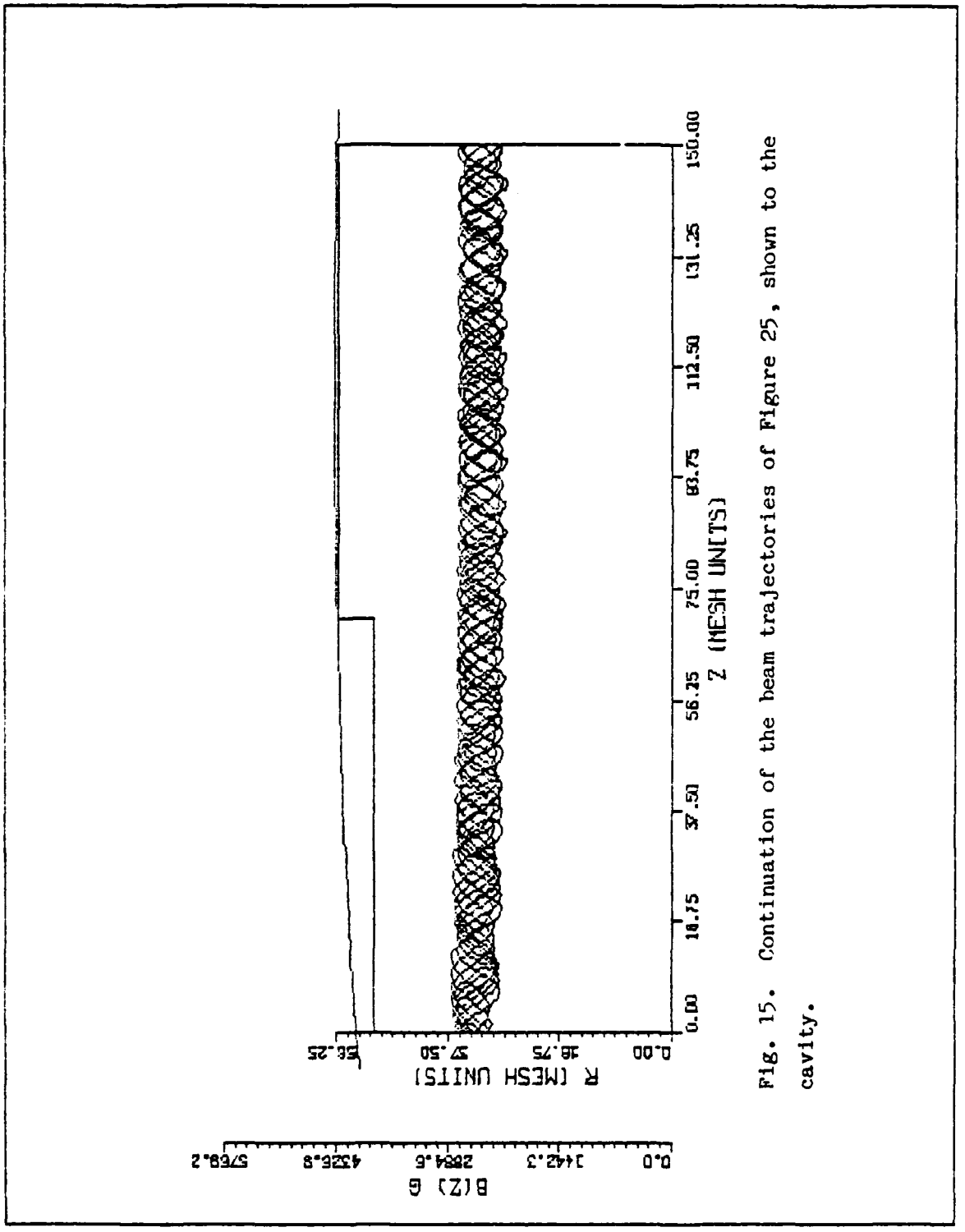

Fig. 15. Continuation of the beam trajectories of Figure 25, shown to the cavity.

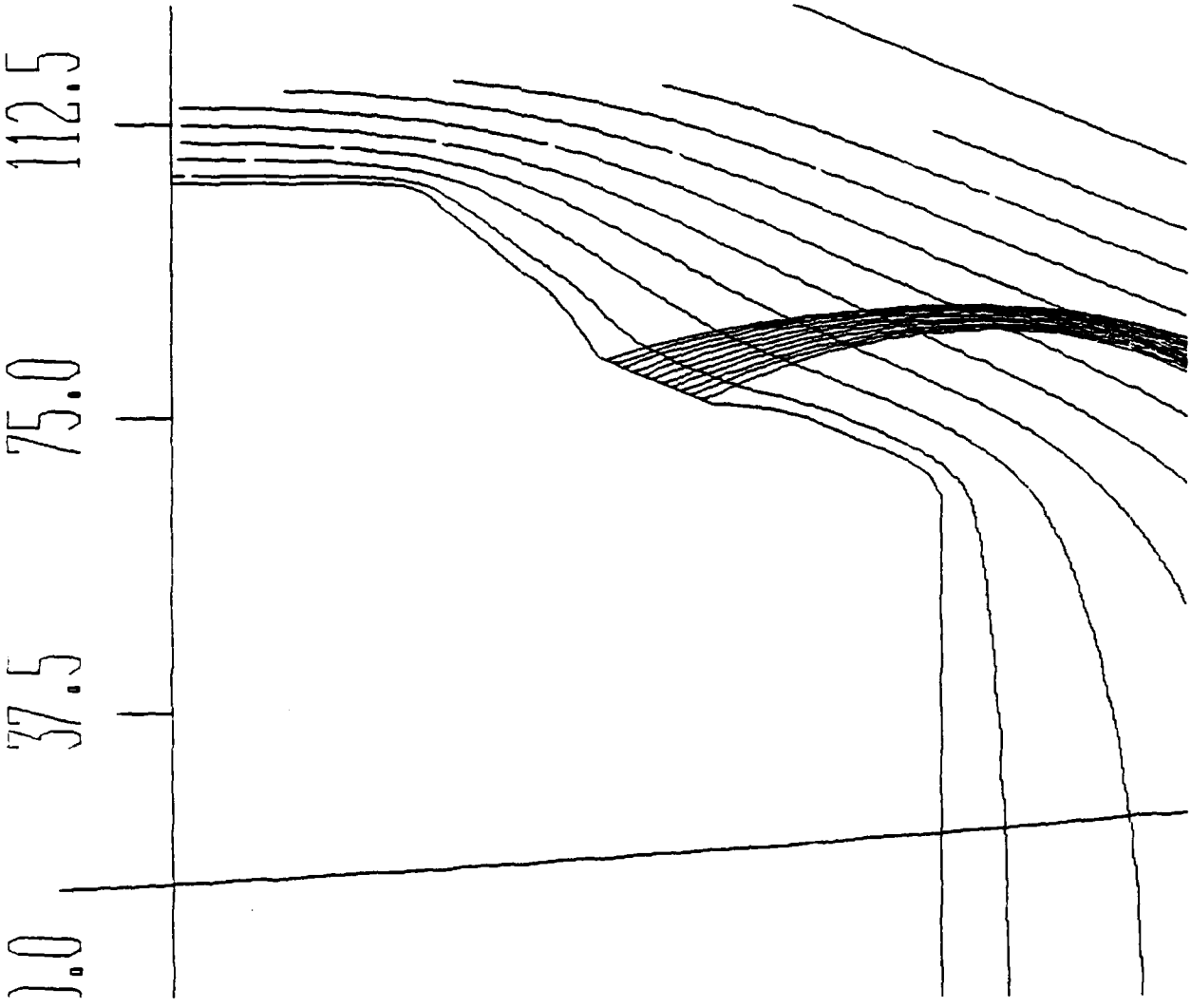

Fig. 16. Enlargement of the region near the cathode of Figure 26.

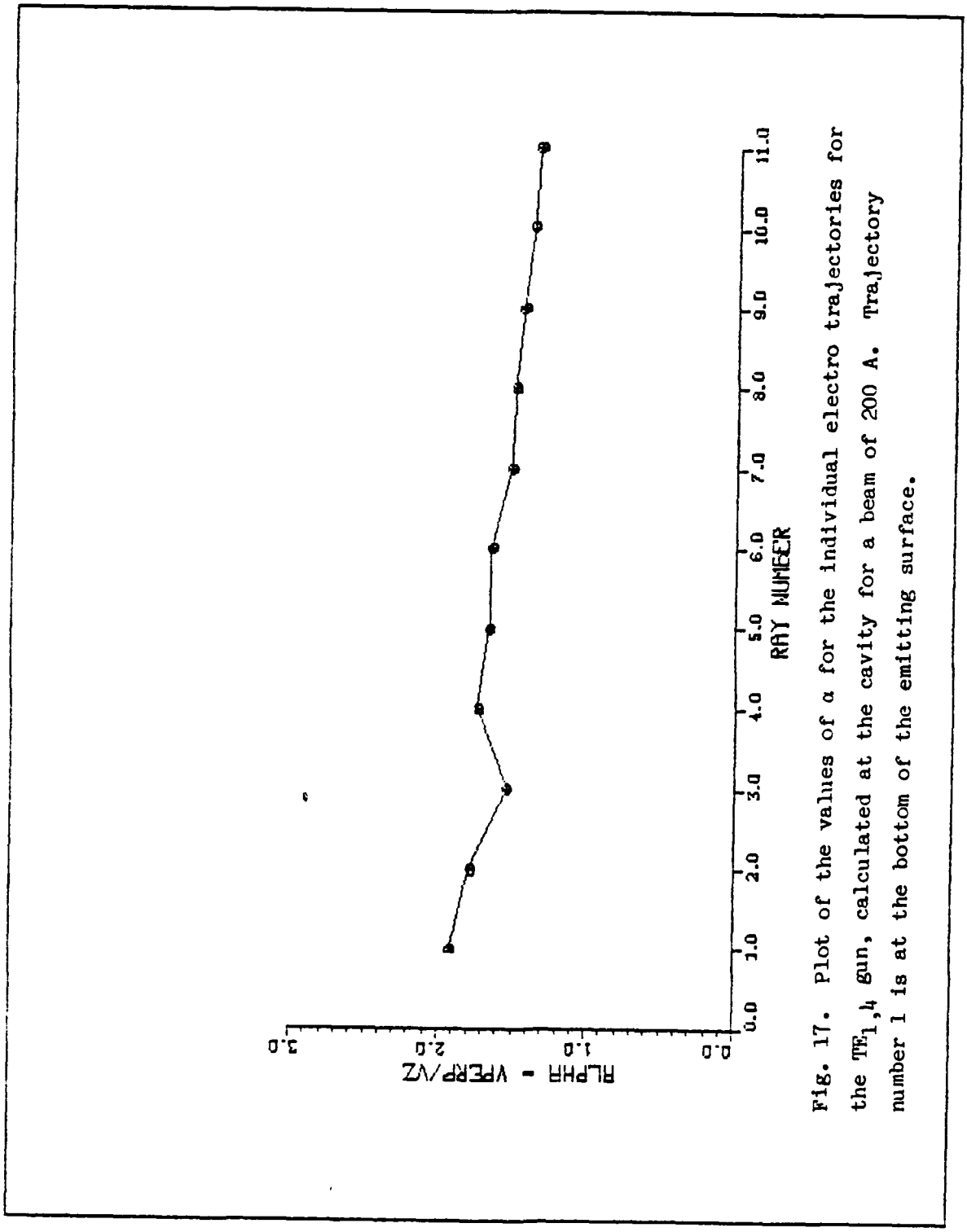

Fig. 17. Plot of the values of α for the individual electro trajectories for the $TE_{1,4}$ gun, calculated at the cavity for a beam of 200 A. Trajectory number 1 is at the bottom of the emitting surface.

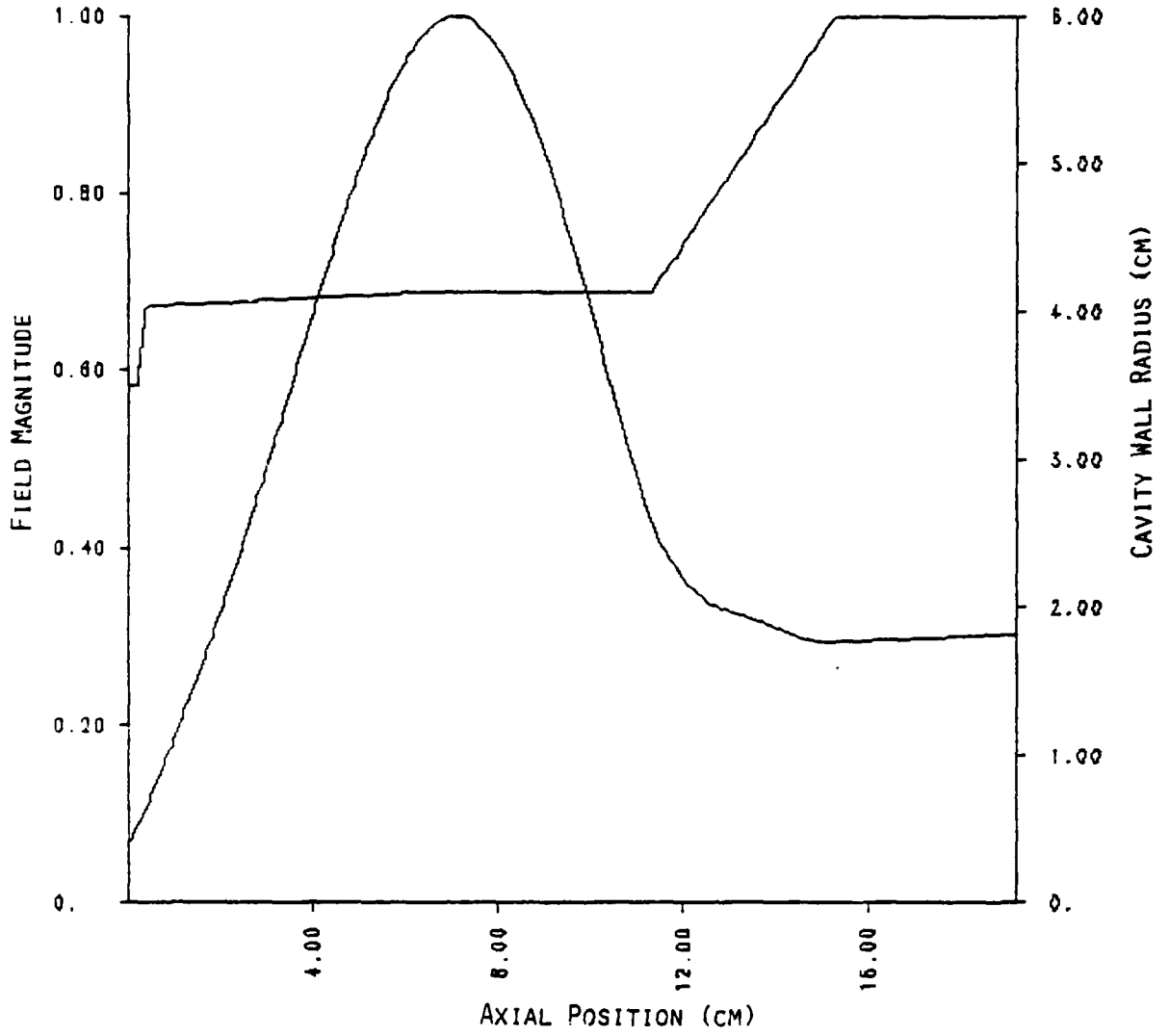

Fig. 18. Schematic of the $TE_{1,3}$ cavity used in the calculations, along with the axial profile of the RF electric field. The dimensions are in centimeters. The Q of the cavity is 200, with a resonant frequency of 9.92 GHz.

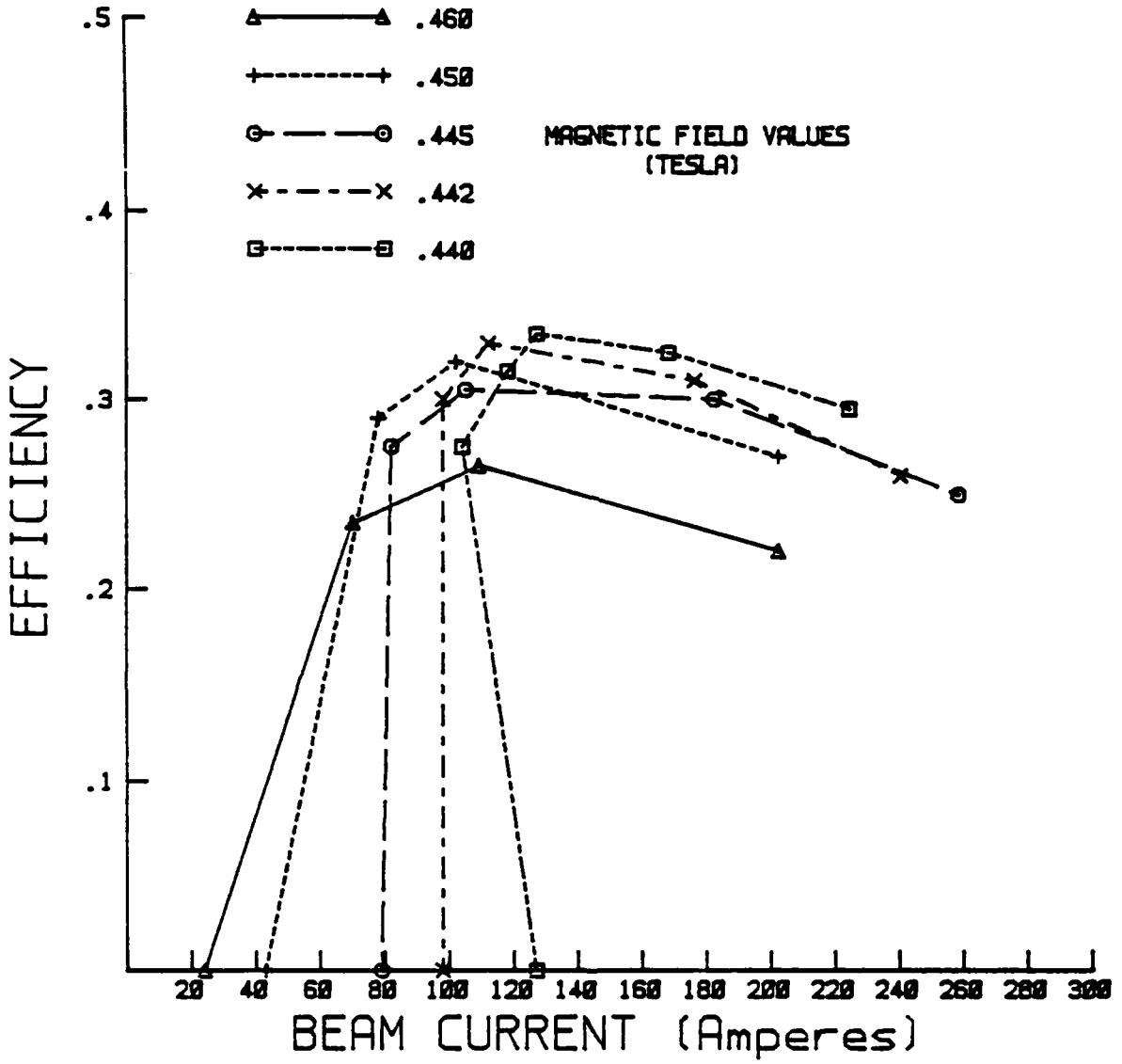

Fig. 19. Results of the calculation of efficiency as a function of current for the $TE_{1,3}$ cavity, using the RF profile of Figure 5. α = 1.5 and V = 218 kV. Zero spread in the beam velocities was assumed. The average beam radius is 1.7 cm.

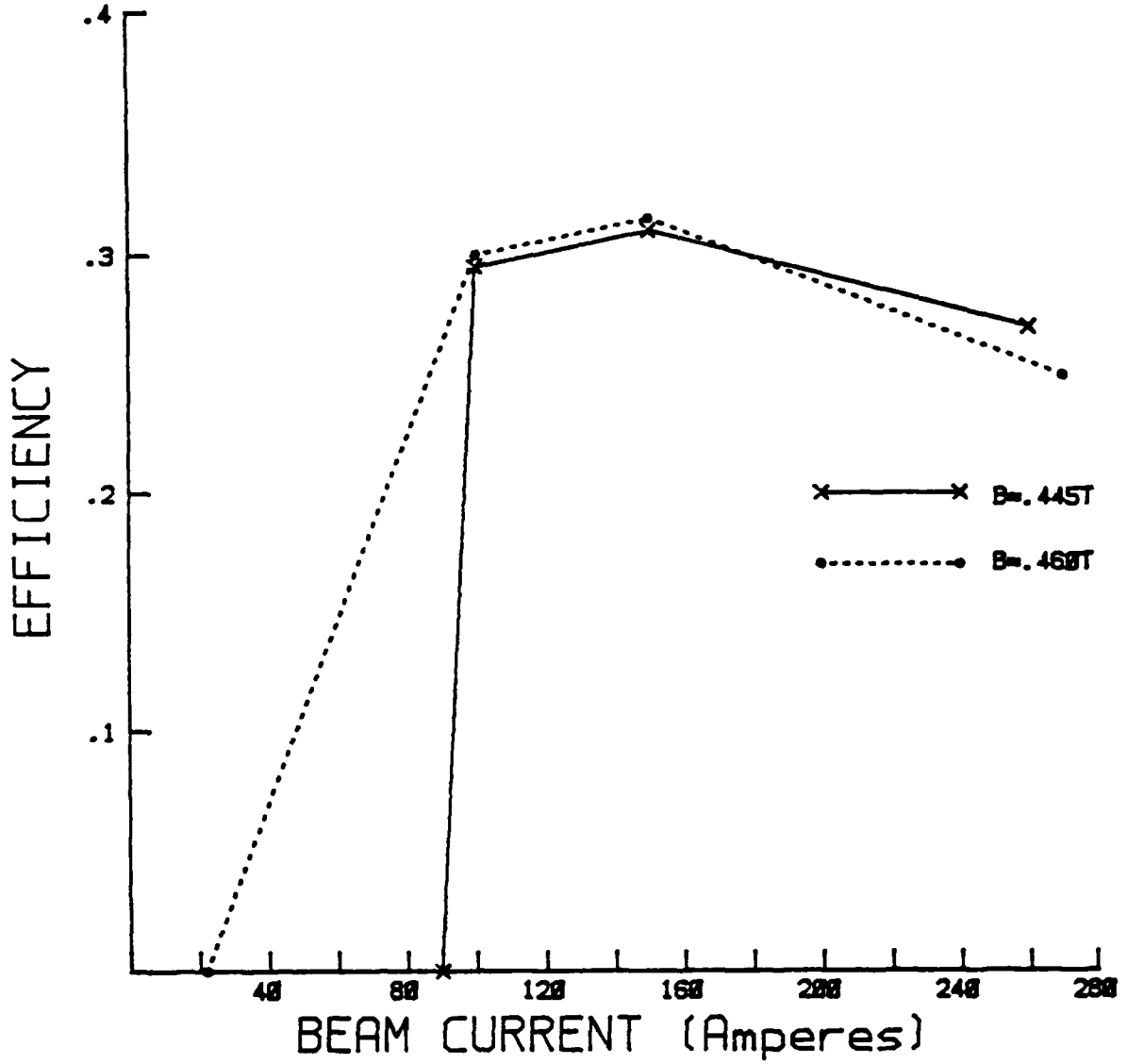

Fig. 20. As Figure 5, but with $\Delta v_{||}/v_{||} = 11\%$.

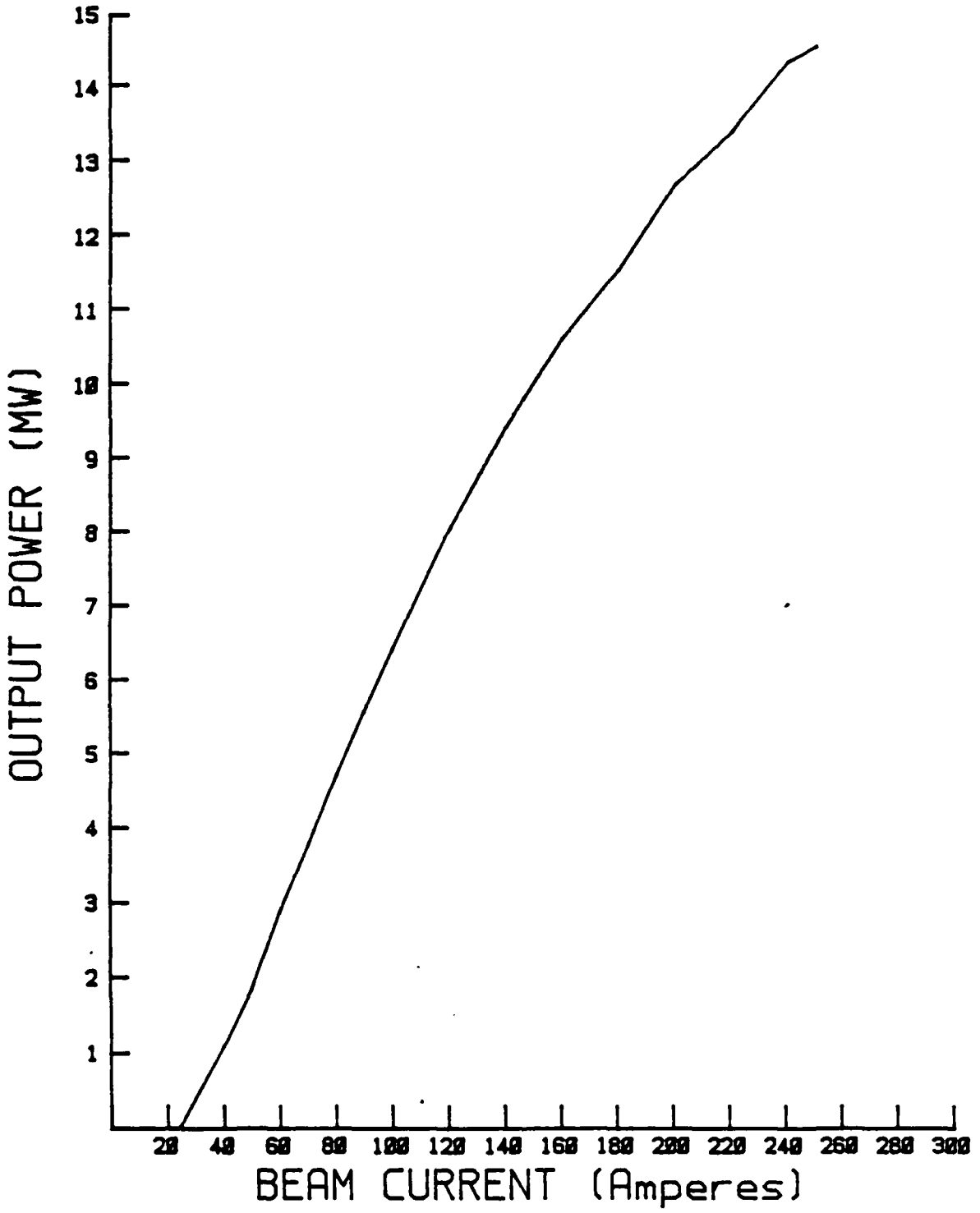

Fig. 21. Plot of output power versus current for the $TE_{1,3}$ cavity of Figure 2, with $\Delta v_{||} = 11\%$.

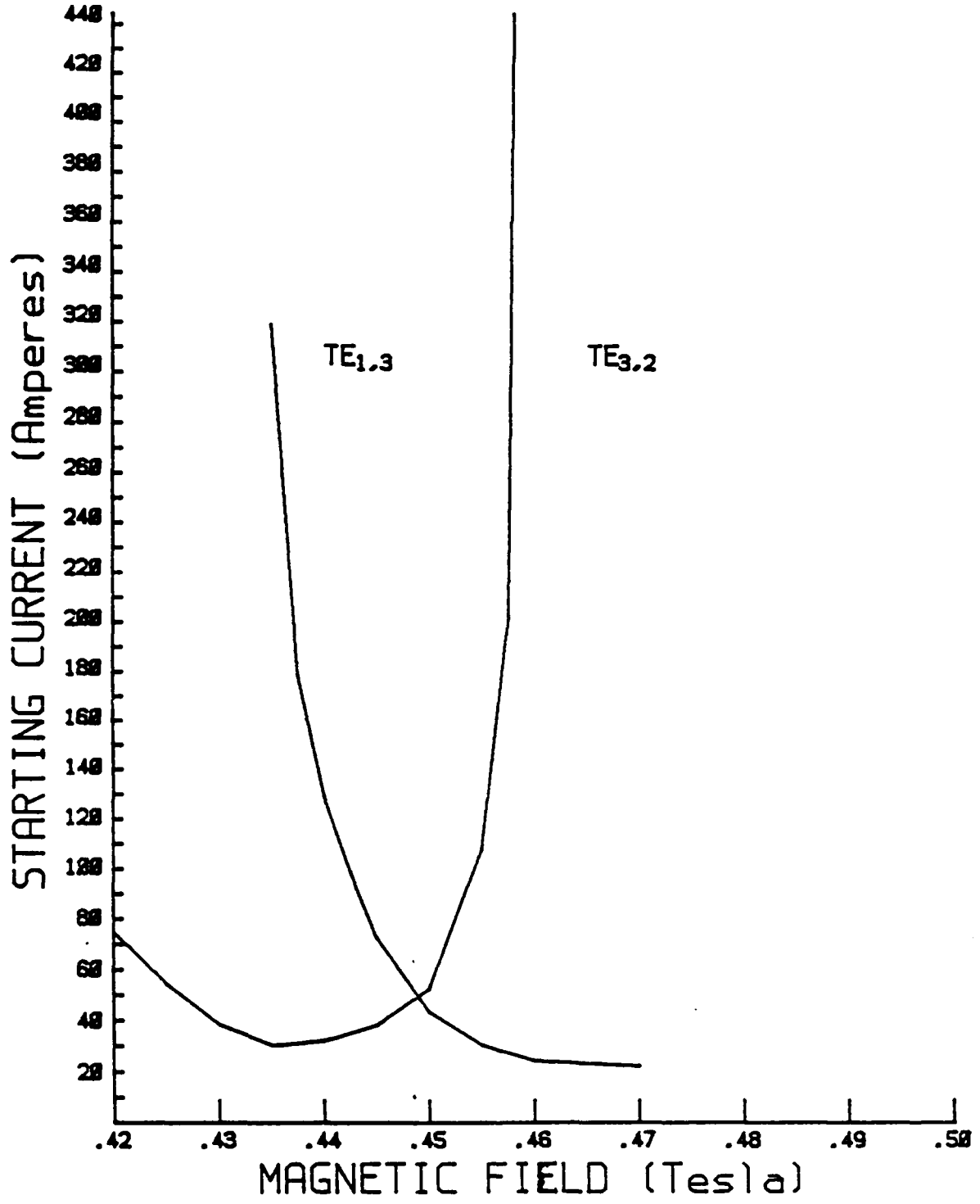

Fig. 22. Plot of the starting current as a function magnetic field, for the $TE_{1,3}$ and $TE_{3,2}$ modes. Calculations were made for other modes, but the starting currents were greater than 400 Amperes over the range of magnetic fields considered.

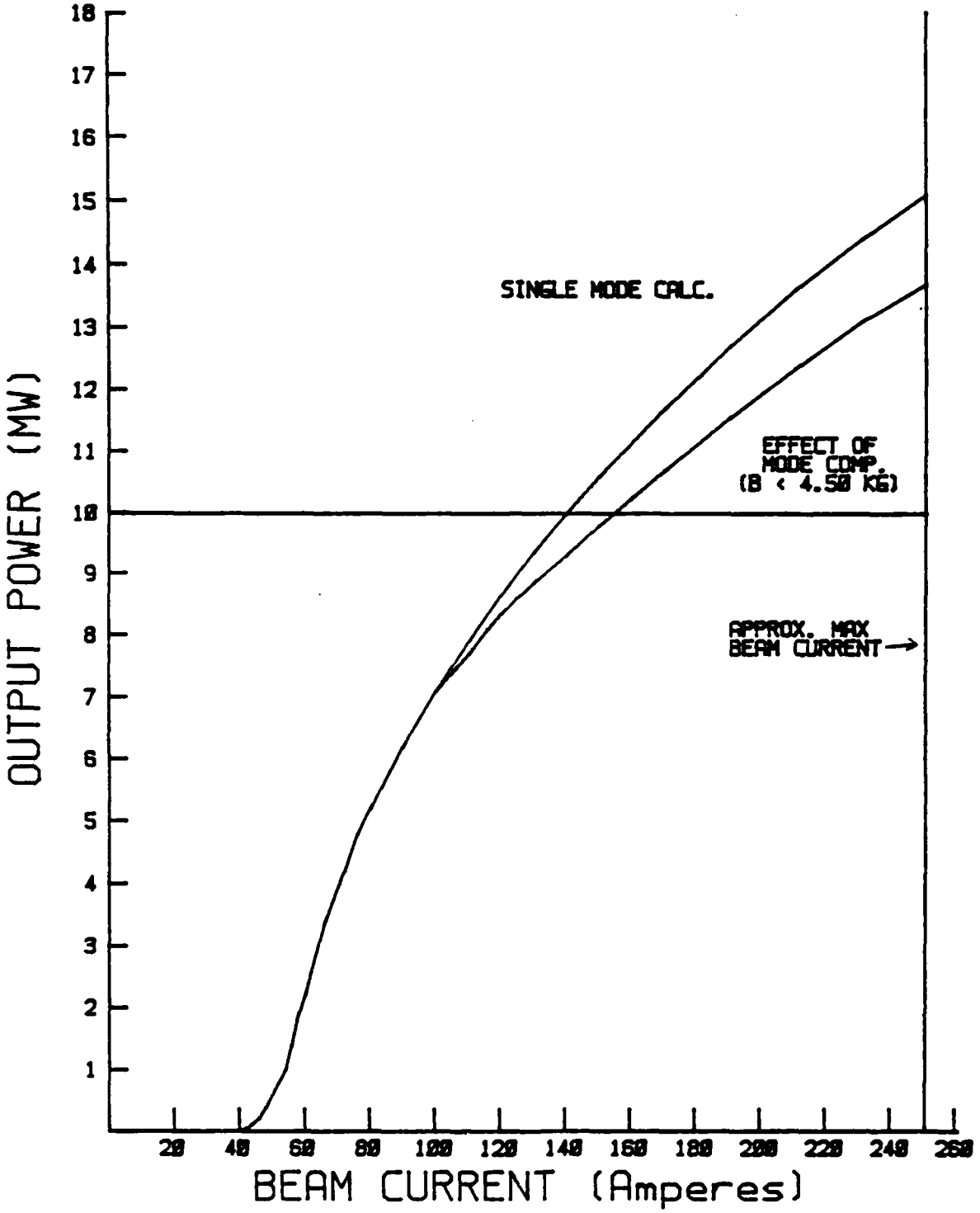

Fig. 23. Plot of output power versus current for the $TE_{1,3}$ cavity, of Figure 5, with and without mode competition ($\Delta\alpha = 0$).

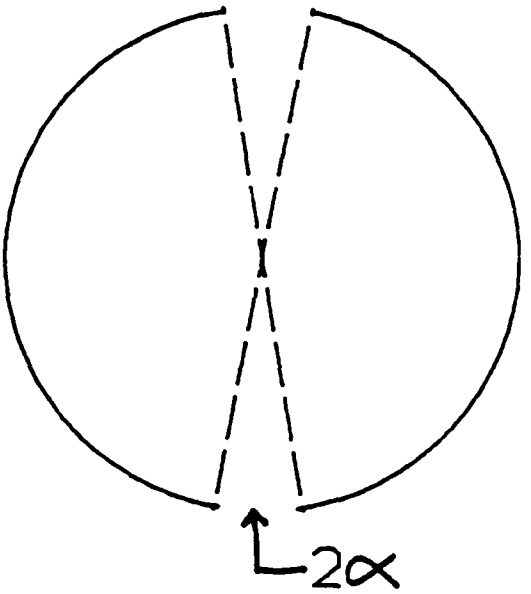

(a)

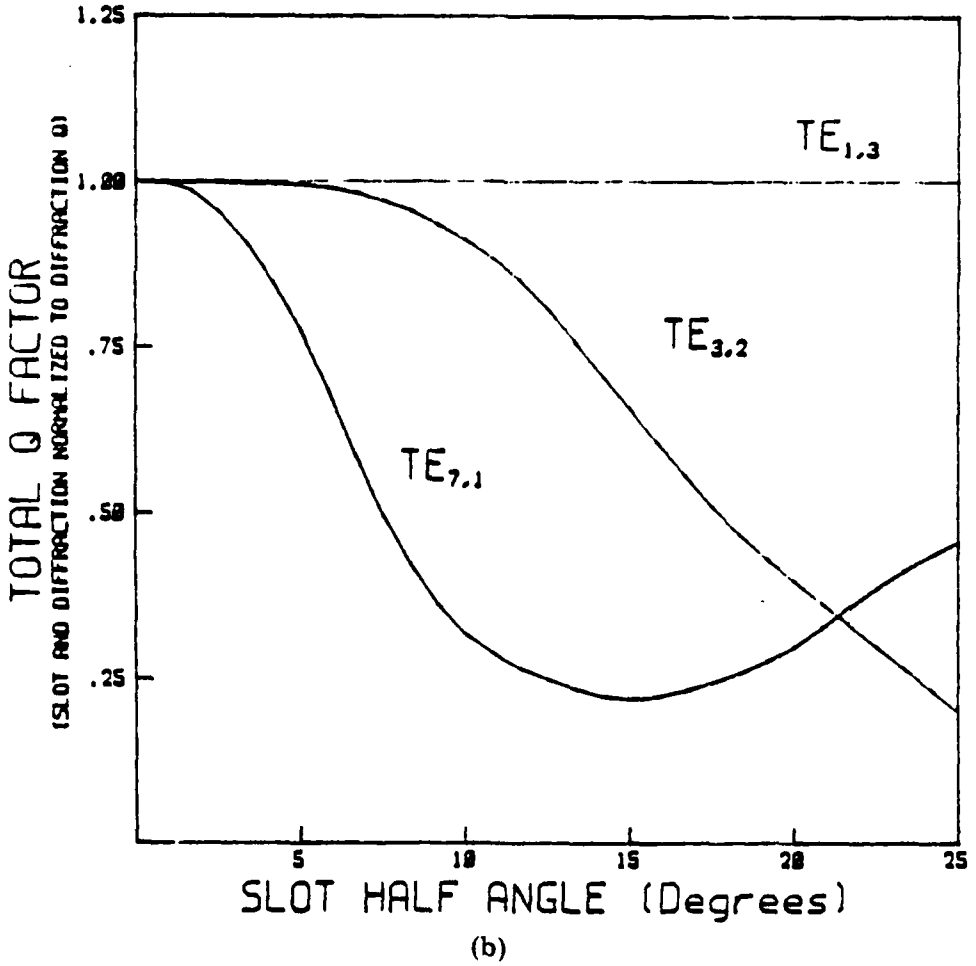

(b)

Fig. 24. (a) Geometry of the calculations of slot Q. (b) Results of the calculations of the Q due to the slots, as a function of slot angle. From A. Fliflet[15].

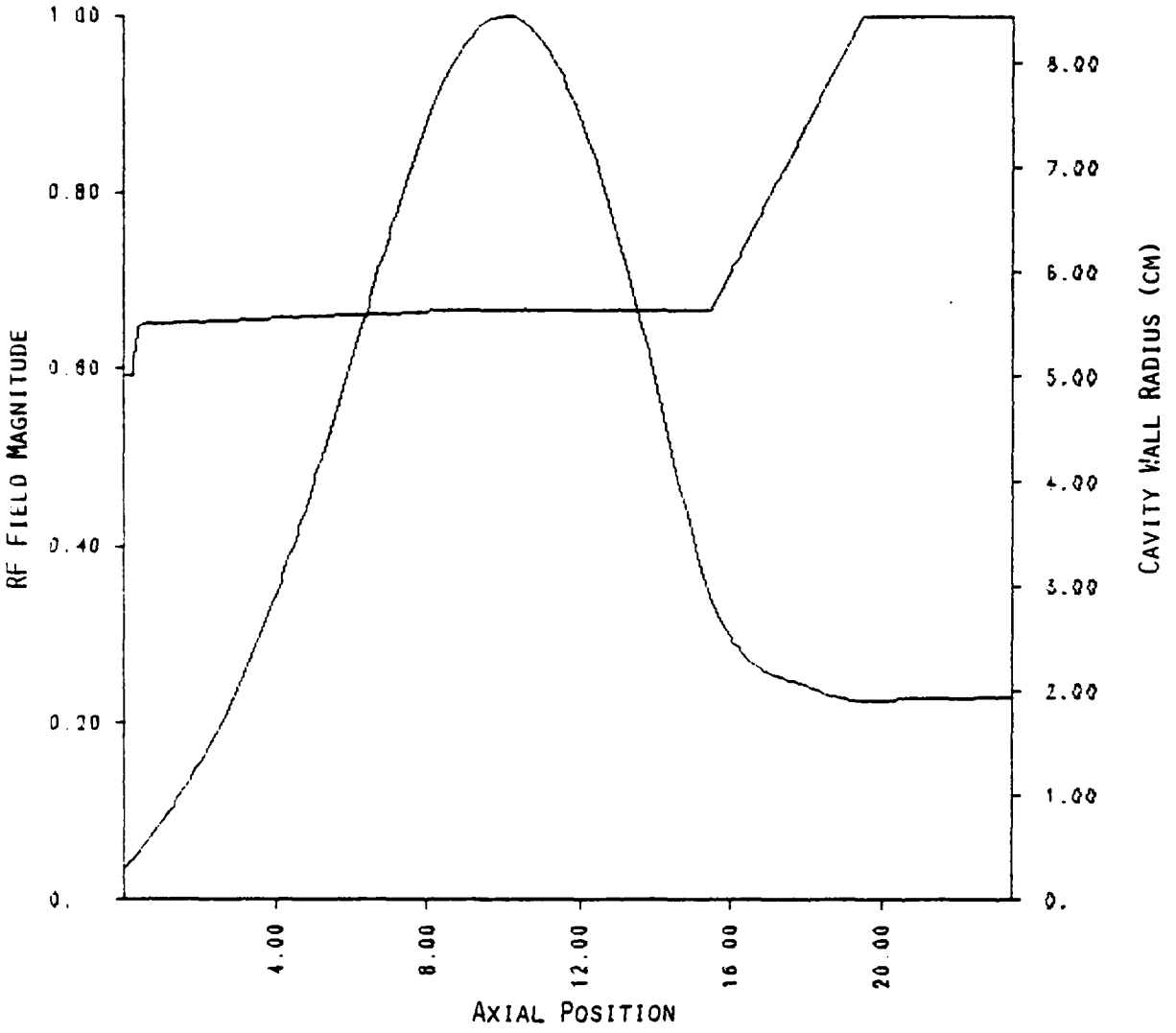

Fig. 25. Schematic of the $TE_{1,4}$ cavity, along with the axial profile of the electric field. Dimensions are in cm. The Q of the cavity is 392, with a resonant frequency of 9.99 GHz.

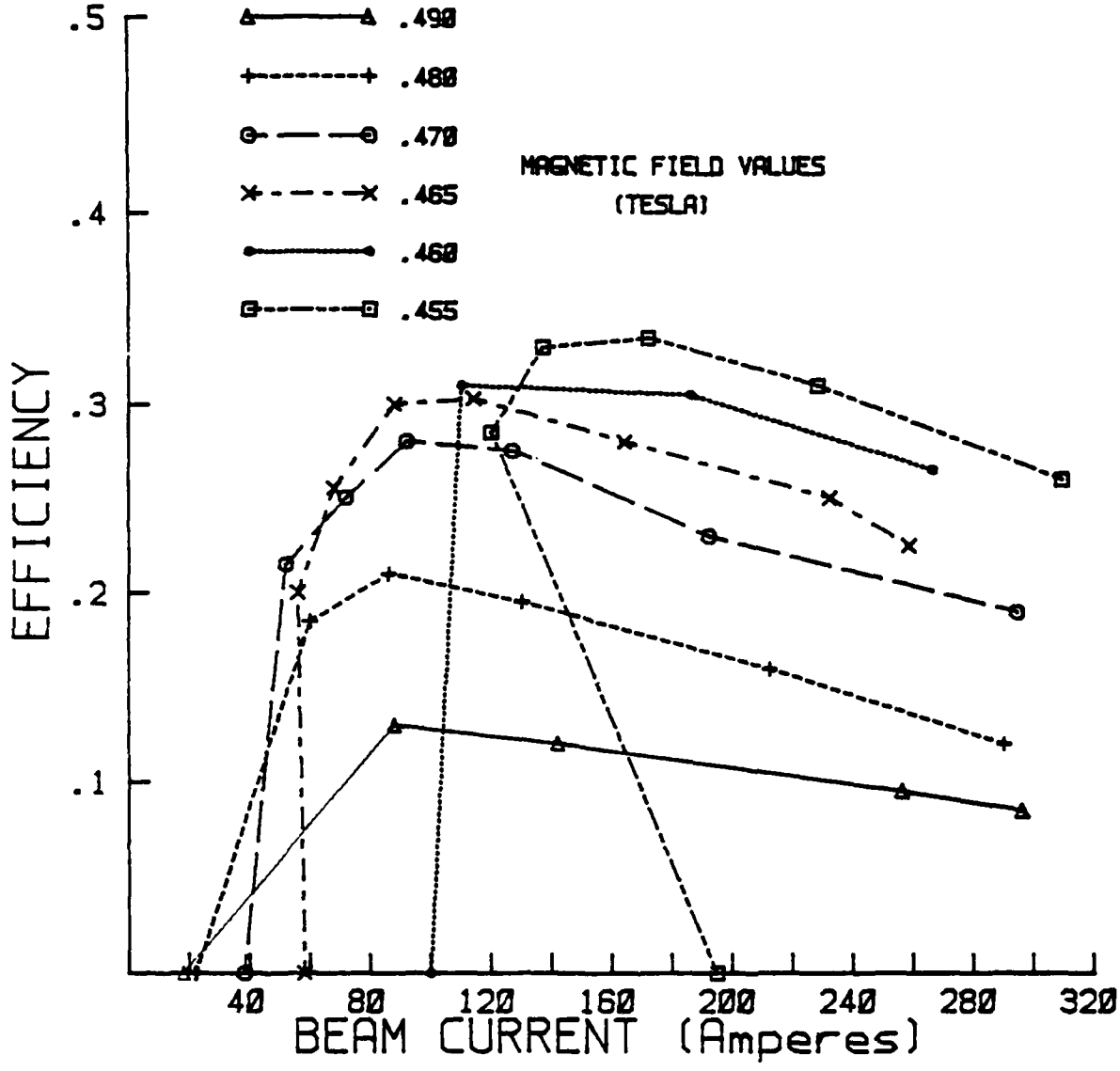

Fig. 26. Results of the calculations of efficiency as a function of current and magnetic field, for the $TE_{1,4}$ cavity, using the RF profile of Figure 9.

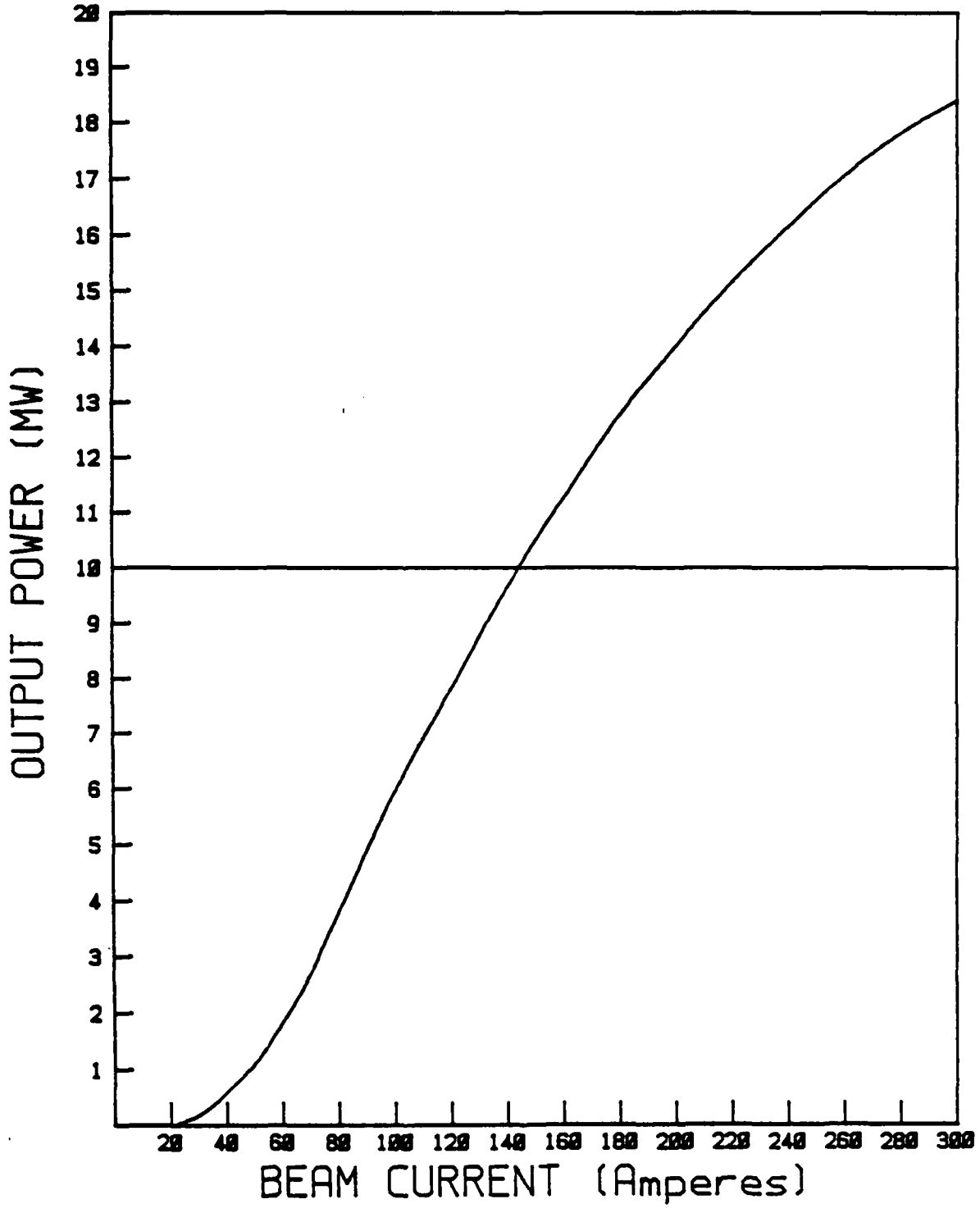

Fig. 27. Plot of power versus current for the $TE_{1,4}$ cavity of Figure 25.

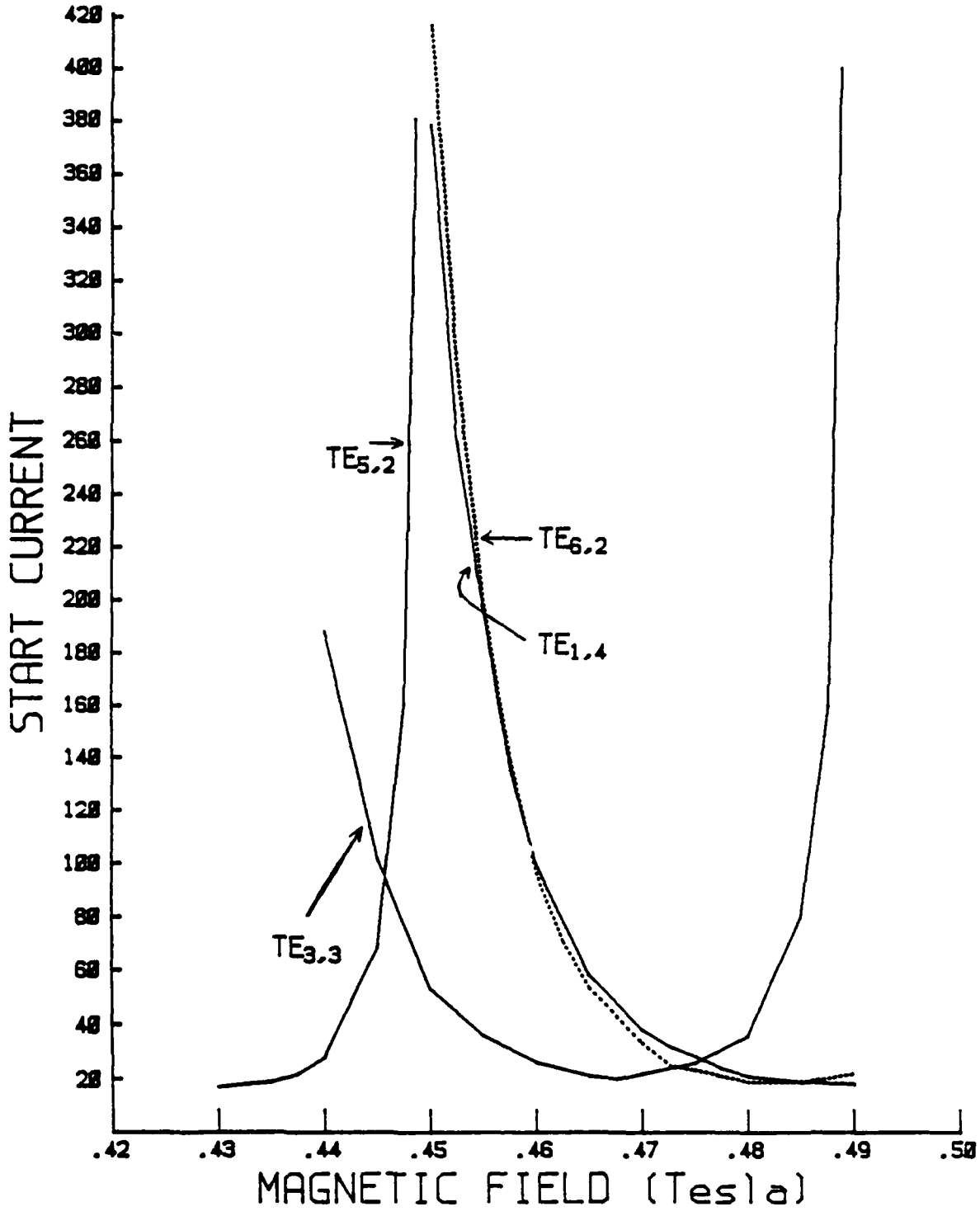

Fig. 28. Plot of the starting current as a function of magnetic field, for the $TE_{1,4}$ $TE_{6,2}$, $TE_{5,2}$ and $TE_{3,3}$ modes.

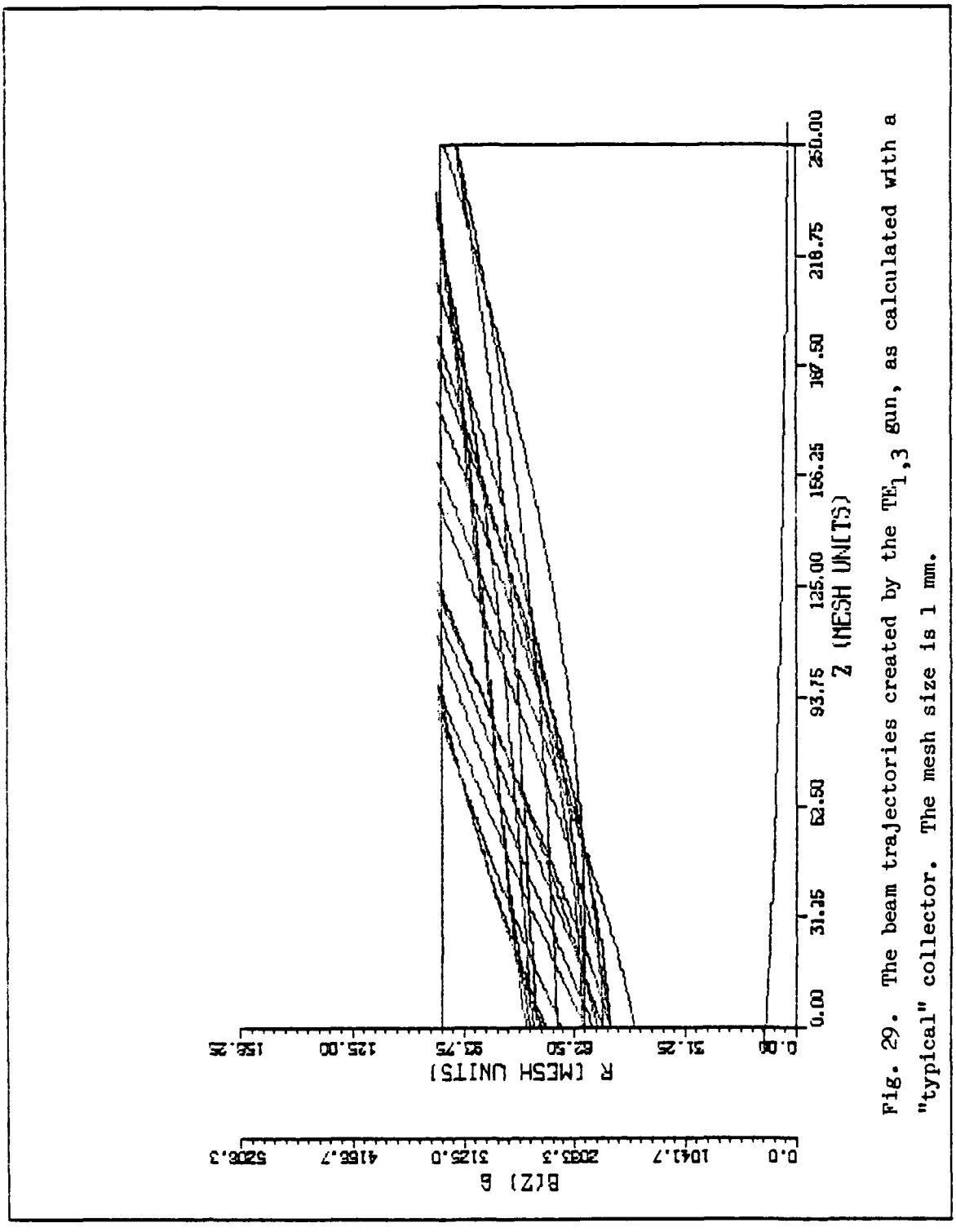

Fig. 29. The beam trajectories created by the $TE_{1,3}$ gun, as calculated with a "typical" collector. The mesh size is 1 mm.

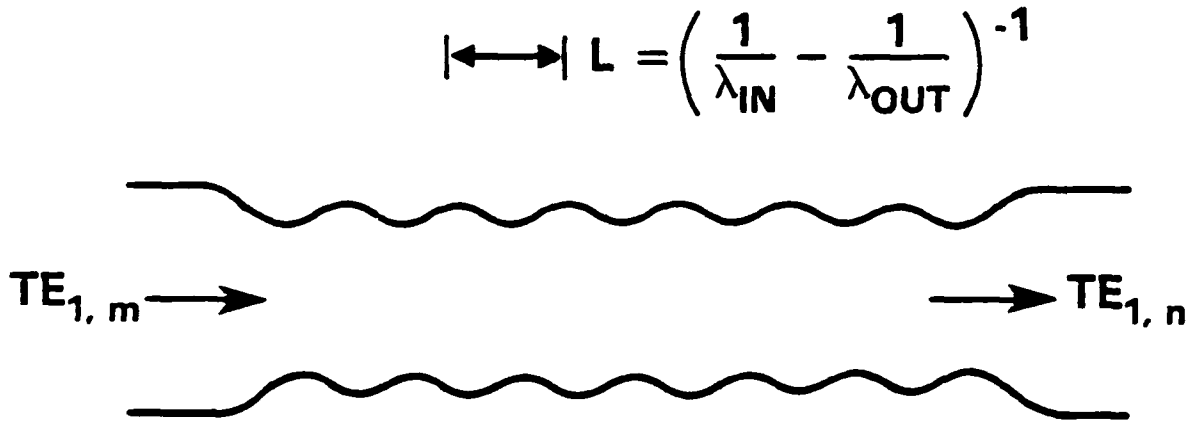

Fig. 30. Geometry of a rippled wall mode converter.

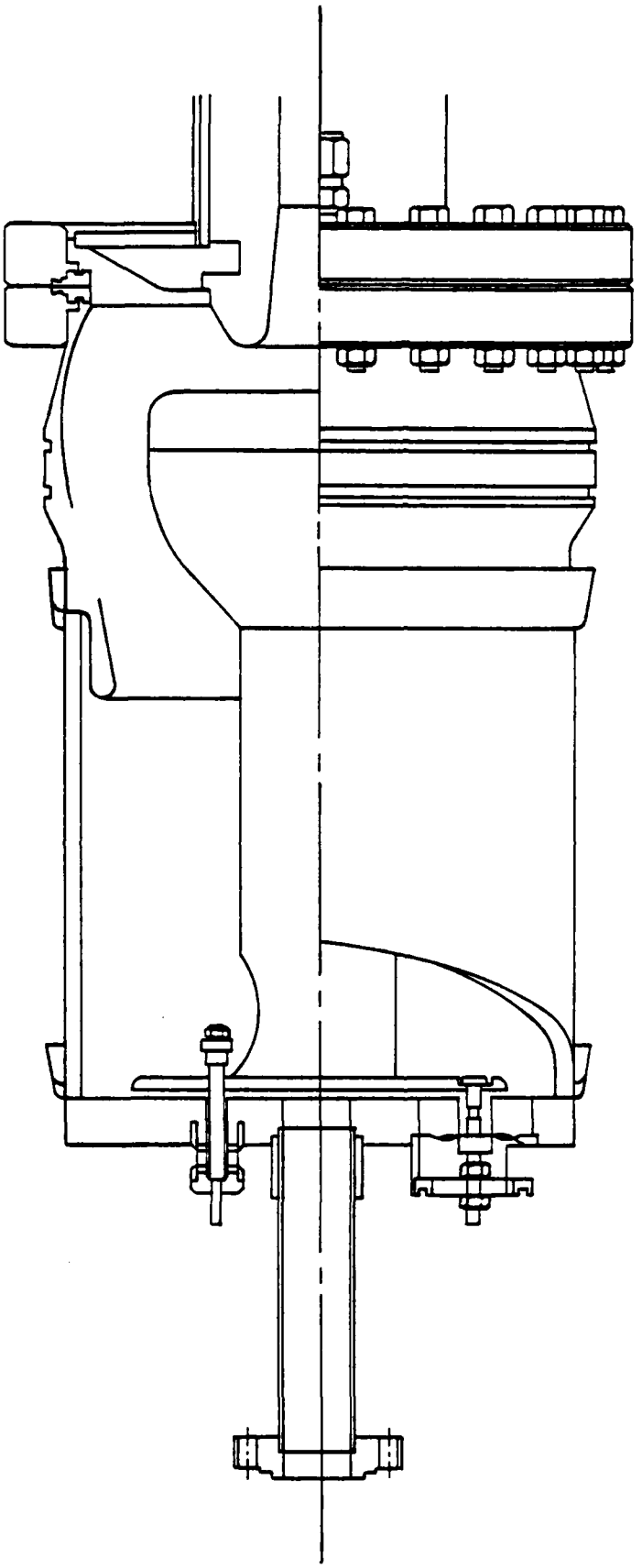

Fig. 31. Diagram of the electron gun assembly from the SLAC 5045 klystron.

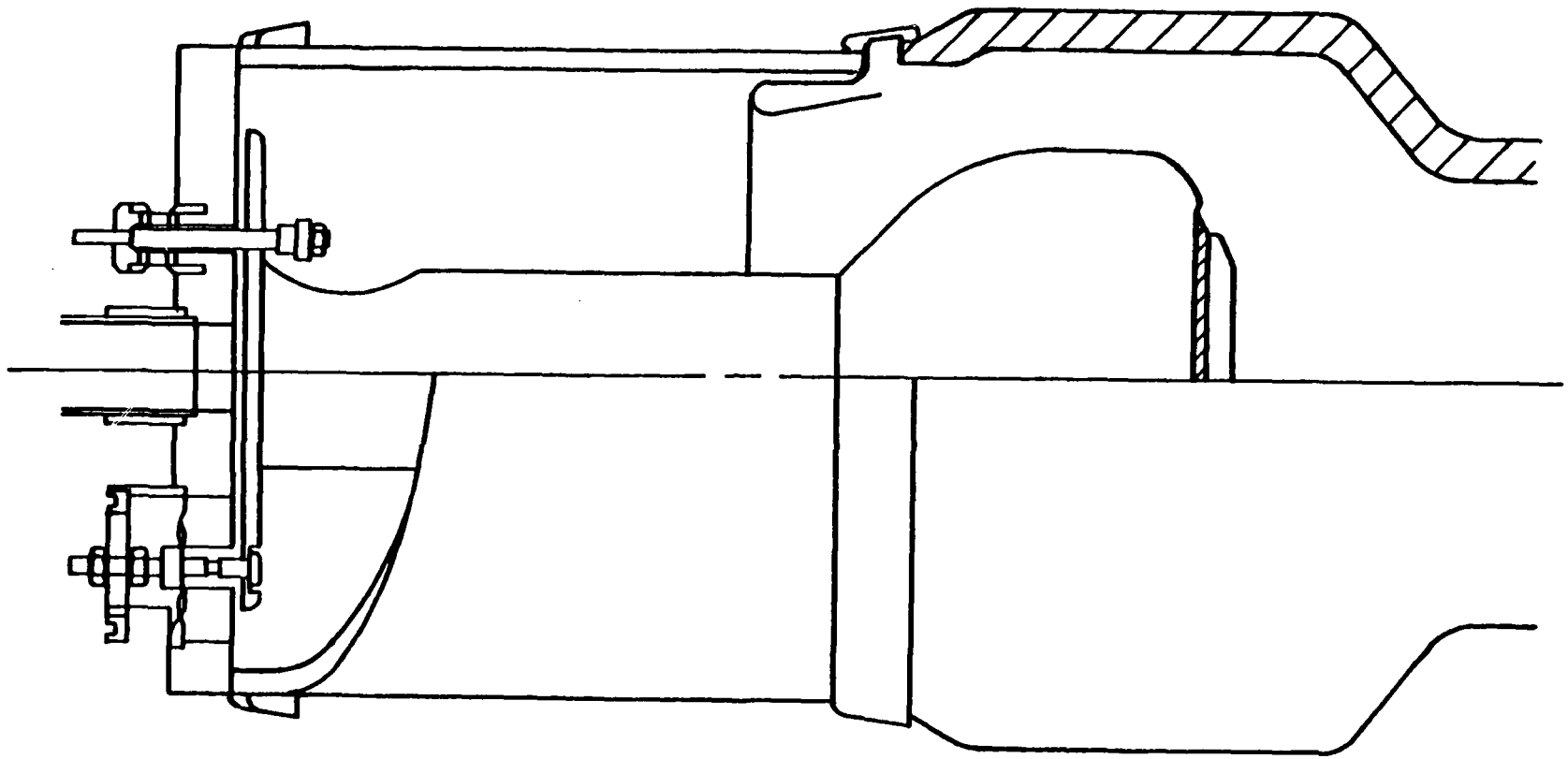

Fig. 32. Diagram of the SLAC gun assembly as modified for use as a gun for the gyrotron.

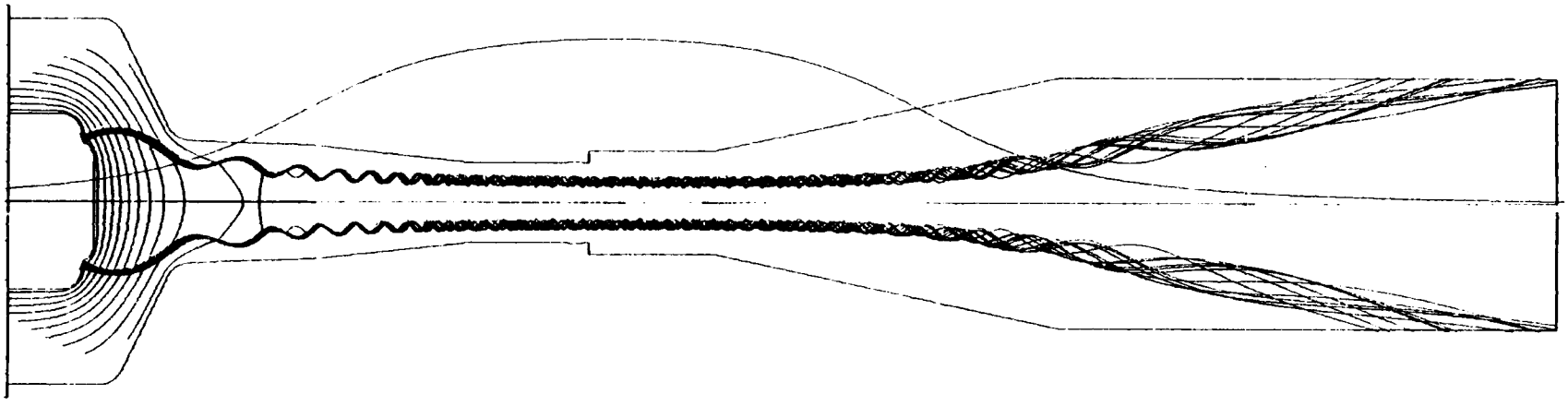

Fig. 33. Composite drawing of the entire gyrotron (less output window). The beam calculation used a 'dummy' magnet. The actual gyrotron will have a larger bore magnet; thus the tube will be longer. The tube as shown is 163 cm long.

References

1. V.L. Granatstein, et al., "Infrared and Millimeter Waves" (K. Button, ed.) 5, pp. 267-304, (1982).

2. Didenko, et al., Soviet Plasma Physics 2, p. 514, (1976).

3. N.S. Ginzburg and G.S. Nusinovich, Isv. VUZ Radiofizika, 22, p. 754, (1979).

4. P. Sprangle, and A.T. Drobot, IEEE Trans. Microwave Theory Tech. MTT-25, pp. 528-544 (1977); E. Ott and W. Manheimer, IEEE Trans Plasma lei, 1, p. 53, (1975); P. Sprangle and W. Manheimer, Phys. Fluids, 18, p. 224, (1975).

5. Y. Carmel, et al., Int. J. Infrared and mm Waves 51, p. 743 (1983).

6. K. Felch, et al., Conf. Digest, Eighth Int. Conf. IR and mm Waves, 14, p. 2 (1983).

7. A.A Andronov, et al., Infrared Phys. 18, pp. 385-393 (1978).

8. S.N. Vlasov, et al., Radio Eng. and Elect. Phys. 20, No. 10, p. 14 (1975).

9. J.S. Levine, Int. J. Infrared and mm Waves, 5, p. 937 (1984).

10. K.R. Chu and R. Lee, unpublished data.

11. M.E. Read, et al., Int. J. of Infrared and mm Waves, 2, p. 159 (1981).

12. A.W. Fliflet, et al., Int. J. Electronics 53, 743 (1982).

13. W.B. Herrmannsfeldt, SLAC-Report-226, (1979).

14. A.K. Ganguly and K.R. Chu, Int. J. Infrared and mm Waves 5, p. 103 (1984).

15. A.V. Gaponov, et al., Fourth Int. Conf. Infrared and Near mm Waves, (1979).

16. A.W. Fliflet, NRL Memorandum Report #5598 (1985). (AD-A157 476)

17. A.W. Fliflet, private communication

18. H.S. Carslaw and J.C. Jaeger, Conduction of Heat in Solids, p.75.

19. L. Pages, et al., Atomic Data 4, p. 1 (1972).

END

FILMED

1-86

DTIC